Available online at www.sciencedirect.com
ScienceDirect
Biochimica et Biophysica Acta 1778 (2008) 1154–1180
Biochimica et Biophysica Acta BBA
www.elsevier.com/locate/bbamem

Characterization of domain instabilities in lipid bilayers by Karhunen–Loeve analysis

Joshua D. Deetz, Roland Faller *, Ahmet Palazoglu

Department of Chemical Engineering and Materials Science, University of California, One Shields Avenue, Davis, CA 95616, USA

Received 19 October 2007; received in revised form 21 December 2007; accepted 28 December 2007
Available online 12 January 2008

Abstract

We study the stability of lipid bilayers with artificial domains. In investigating different domain structures, we identify scenarios of stable and unstable arrangements of patches of mixed phospholipids. These are then characterized using Karhunen–Loeve Expansion (KLE), a special form of Principal Components Analysis (PCA). The simulation data are interrogated using KLE to reveal spatiotemporal patterns that explain relevant motions in the bilayer system. By projecting the high-dimensional dataset onto a small number of key modes, KLE reveals specific dynamic signatures that can help distinguish and characterize various domain instability mechanisms. We find that typically very few modes are responsible for describing a mechanism of instability to a reasonable extent and can clearly distinguish between stable and unstable arrangements. Different instability modes are characterized as they exhibit unique features like global deformation or local mixing modes.

Keywords: Principal component analysis; Lipid bilayer; Molecular simulation; Pattern formation

1. Introduction

Phospholipid bilayers have become a popular topic of study in recent years due to their importance in biological systems [1–3]. Membranes on organellar and cellular scales consist of mixtures with a wide variety of lipids and proteins. Membrane properties such as domain formation play important roles in many cellular functions and intercellular chemistry. Biologically relevant concentrations of lipids form a number of heterogeneous shapes and patterns including stripes and circular phases. The most biologically relevant phase is the fluid lipid bilayer. At lower temperatures, the tails of lipids protract inwards to allow for a tightly packed structure, a gel-like phase. It has been observed that lipids which have longer tails prefer the gel phase and leave the shorter components in the fluid phase. All bilayer phases are members of the smectic liquid crystalline phase family [4,5]. Rafts, i.e., patches of highly ordered but still fluid lipids and embedded proteins, can aggregate and are vital to cell signaling [4,6]. Consisting primarily of sphingolipids and cholesterol, these small patches in the bilayer coexist with less densely packed membrane areas. Due to the small size and short lifespan of raft domains, owing to the fluctuating nature of the bilayer system, their experimental study is problematic. Thus, simulation has become an invaluable tool for traversing the biological energy landscape. Historically, simulations were limited to an inconsequential number of atoms with a simulation time of at best a few nanoseconds [7]. Advances in computer hardware and simulation techniques have unlocked new territories for research. As a result, the number of particles and the length of simulations that are possible today have greatly broadened [8]. The majority of computational studies on bilayer systems have focused on local molecular dynamics in full atomistic detail [9–15]. This restricts the size and time scales of simulations such that no information regarding phase behavior can be obtained. Coarse-graining (CG) techniques that average some of the properties of neighboring atoms into larger units or super atoms have been developed so that greater timescales and numbers of particles can be simulated [16–23]. This procedure condenses the information of several atoms into a single particle that interacts with others typically through short-range potentials. The Martini force-field [17,18] is one such CG method that uses simplified

* Corresponding author.
E-mail address: rfaller@ucdavis.edu (R. Faller).

0005-2736/$ - see front matter © 2008 Elsevier B.V. All rights reserved.
doi:10.1016/j.bbamem.2007.12.027

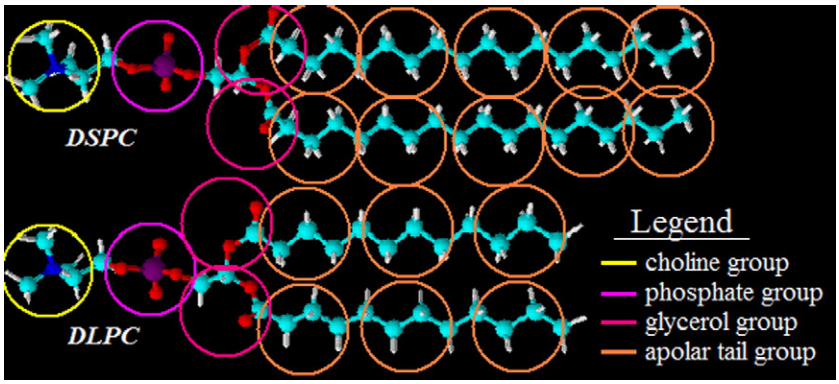

Fig. 1. Illustration of chemical structure and bead orientation of DSPC (top) and DLPC (bottom). The encircled atoms constitute coarse grained units. Note that the choline group has a positive charge and the phosphate group has a negative charge making both of these groups polar, the glycerol groups are nonpolar, and the tail groups are all apolar.

models between particles and quantitatively compares with experimental data to reproduce such properties as bilayer thickness and area per headgroup [17].

Studying phase changes of a lipid bilayer system involves sorting through vast amounts of data making it difficult to extract meaningful information and to pinpoint mechanisms. Karhunen–Loeve expansion (KLE), a special case of Principal Components Analysis (PCA) [24] can be applied to two-dimensional data sets which vary in both space and time to reveal the most important dynamical features of a system [25]. In a recent study, we have applied KLE to a phase separating mixture of lipids and characterized the changes that occur in the local concentrations in a bilayer, demonstrating that KLE is capable of qualitatively describing domain formation [26]. However, an artificially structured bilayer system has never been studied using this method. In this paper, we seek to apply KLE to bilayer systems to characterize the primary mechanisms by which changes in the domain structure occur in a mixture of di-lauryl and di-stearoyl phosphotidylcholines. We study four systems with different concentrations of 1,2-Distearoyl-*sn*-Glycero-3-phosphocholine (DSPC) and 1,2-Dilauroyl-*sn*-Glycero-3-phosphocholine (DLPC) [16,27]. KLE is used to reveal the dominant motions leading to phase decomposition in bilayers with several distinguishing features such as circle and stripe patterns, undulations, and uneven concentrations of species in bilayer leaflets. In short, we seek to apply the KLE to elucidate factors that lead to structural deformation in mixtures of DSPC and DLPC for a bilayer system.

2. Methodology

2.1. Simulations

Simulations were performed with the Gromacs (V 3.2) Simulation Suite [28]. We focus on mixtures of two phospholipids which differ only in the length of their tails. DSPC is six saturated carbon atoms longer than DLPC. We choose this mixture to compare with previous experimental results [29,30] and thus we expect phase separation with DSPC being more ordered and to prefer the gel phase more than DLPC. The lipids were modeled using the Martini [17,18] CG approach where several heavy atoms and their hydrogens are merged into a single particle that interacts with its surroundings via Lennard–Jones short-range potentials and screened electrostatics. Details of the simulations are published elsewhere [16,27]. Here, we summarize the main characteristics. A DLPC molecule contains ten interaction sites whereas DSPC consists of fourteen particles. Each lipid has two oppositely charged polar sites for the headgroup: a positively charged choline group, and a negatively charged phosphate group. Two sites modeling the nonpolar glycerol groups are attached to the headgroup, and three or five interaction sites correspond to each of the hydrophobic tails. Fig. 1 illustrates the interaction sites of each lipid and the atoms they correspond to. To emulate the conditions of a biological environment, eleven water molecules were added to the system for every lipid. CG waters correspond to groups of four atomistic molecules, we use the original parameterization from the older version of the Martini model, i.e. water is modeled by only one type of polar particles [17]. This model allows a time step of 160 fs, note that all times are rescaled by the standard scaling factor of 4 for this model. Temperature and pressure were maintained using Berendsen's weak coupling method with a coupling constant of 4 ps [31]. Anisotropic coupling was used for pressure to accommodate independent changes of bilayer area and thickness under orthoromic periodic boundary conditions. Four different systems are studied with varying domain structure and concentrations. Table 1 summarizes the simulation details. The leaflets have generally been analyzed separately.

Table 1
Details of molecular dynamic simulations

System	#DLPC top	#DLPC bottom	#DSPC top	#DSPC bottom	Simulation time (ns)	Area of Simulation box (nm^2)	Temperature (K)
1	528	528	328	328	145	419	385
2	200	328	128	0	202	193	295
3	800	800	100	100	661	455	295
4	150	150	100	100	704	129	285

The simulation time noted here only reflects the time used in the analysis. Actual simulation runs are typically longer [16,27]. Note that we did not rescale times by the customary factor of 4 here [17].

2.2. Decoupling of layers

Separating the two leaflets of a bilayer in an automated fashion is non-trivial. For a flat bilayer in the *xy* plane, the scalar product of the unit *z* vector with the direction vector of the lipid, i.e. the vector that points from the tailgroup to the headgroup should reveal to which layer a lipid belongs. If this product is positive, the lipid is assigned to one layer and vice versa. During the course of the simulation, undulations in the bilayer may hamper determining the direction of the lipid. In some cases, the tails of lipids may curl close to or even above the headgroups resulting in a misaligned vector. Two methods were used to separate leaflets in bilayers. The first method, although primitive, simply subtracts the *z* coordinates of the headgroup and the end of the tail in the first time step. This method is insufficient for layers which misplace their headgroups due to periodic boundary conditions in the first time step. In the case that this occurs, an alternate method of layer separation is required. Generally, as long as the headgroups from one layer do not migrate between the two *xy* planes in the *z* direction, it is a trivial

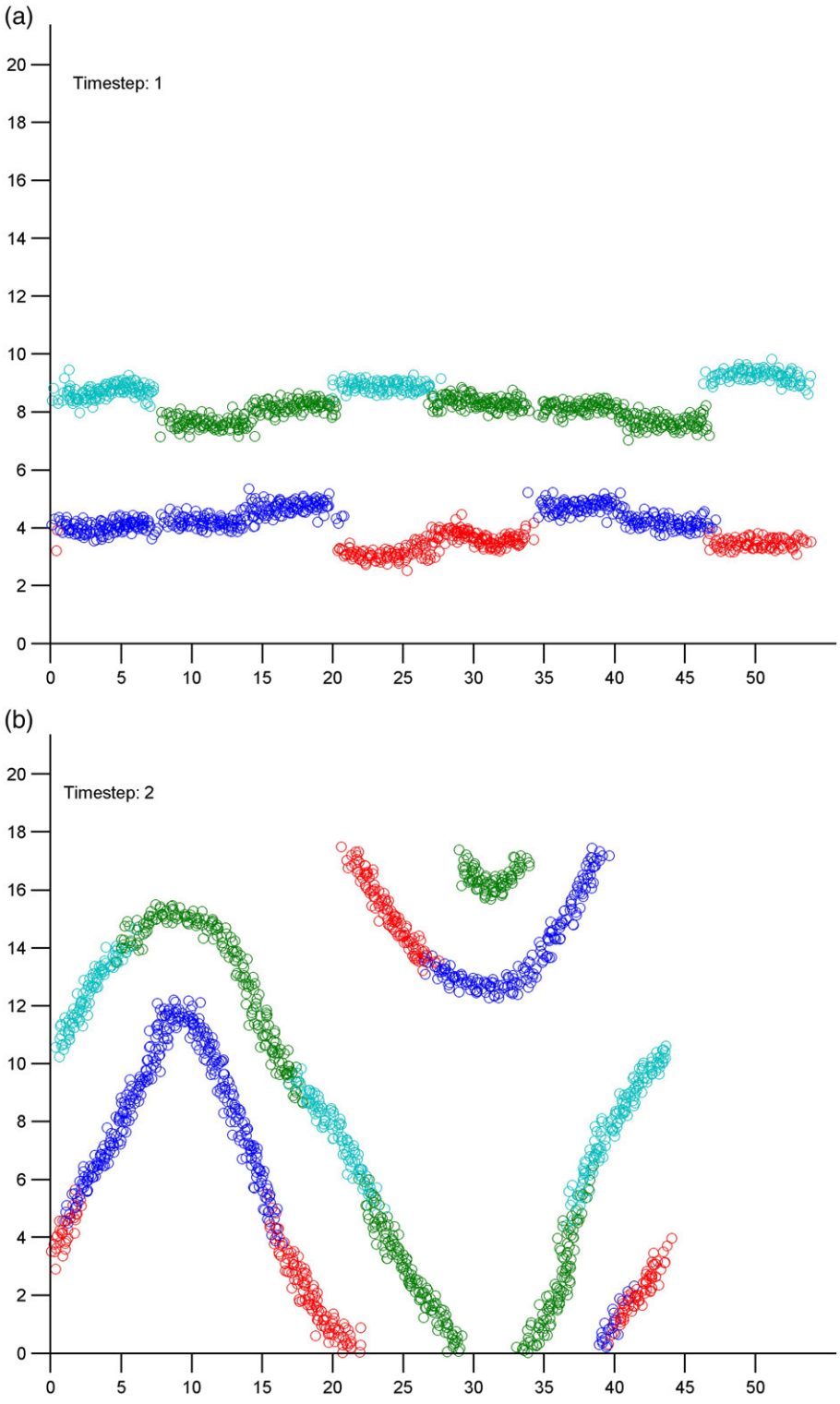

Fig. 2. Changes in the conformation of the 1st bilayer over course of simulation (side-view).

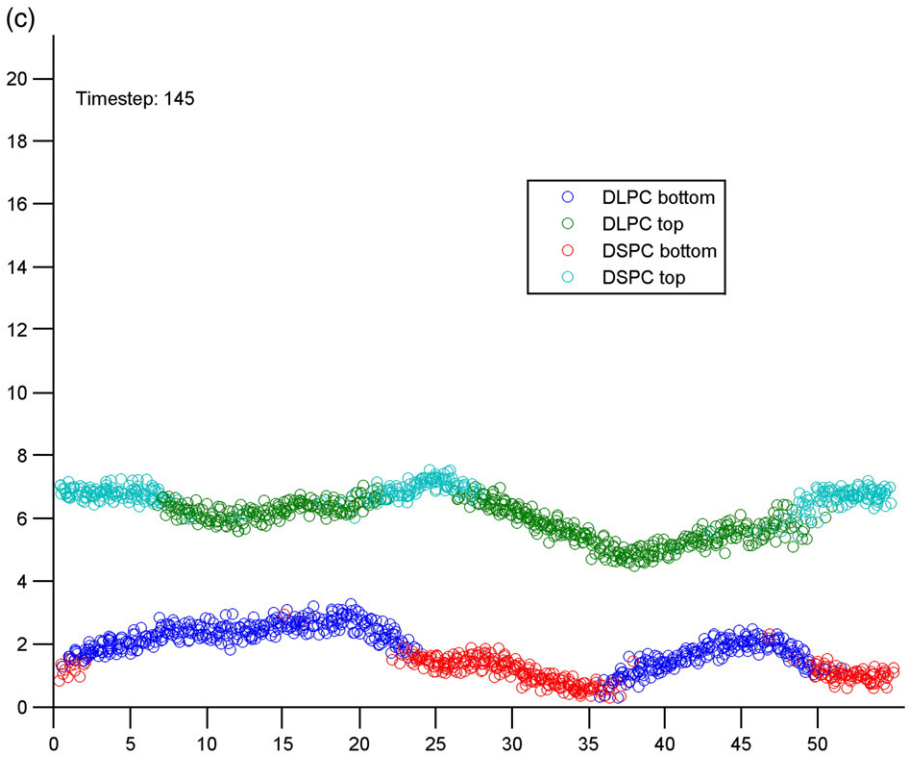

Fig. 2 (*continued*).

matter to differentiate the data corresponding to the top and bottom layer. In the paper, with some abuse of the geometric nomenclature in free bilayers, we will refer to the two leaflets as top and bottom for convenience.

2.3. Karhunen–Loeve Expansion (KLE)

KLE, also often referred to as Principal Components Analysis, is a method of data reduction which expresses a spatiotemporally varying (two-dimensional) set of data using a few dominant modes [25,32,33]. The key idea behind KLE is the projection of a high-dimensional dataset onto a small number of orthogonal directions that explain the majority of the structural (non-random) information. This often results in a significant dimensionality reduction that summarizes the underlying physical phenomena and facilitates their detailed study. In the KLE application here, first the data from the simulations are separated by lipid species and leaflet such that four sets of data are acquired for each simulation. The data contain the x and y positions of a characteristic site for the lipid, the PO4 group in our case. Next, a rectangular grid is drawn along the simulation box in the x and y dimensions where each gridspace corresponds to a fixed location in space. These grids were not rescaled according to constant pressure. The number of lipids in each grid is recorded, producing a local number density. Note that it generally does not matter how the gridspaces are shaped as long as they encompass all of the lipids in the simulation and they are neither too small nor too large [26]. This yields a three-dimensional set of data: the number density in each gridspace as a function of the x and y directions and the current time step. To transform this into a two-dimensional set required by KLE, the x and y directions are compounded into a single index referring to a grid number. This is done by unraveling the gridspaces to form a single direction by capturing all of the elements of the first row in the x direction and then the second row and so on just like how a television writes pixels onto a screen [26]. This yields a matrix $\boldsymbol{P}$ of dimension $I\times J$ where I is the number of gridspaces and J is the number of time steps. The elements of this matrix are number densities on grid points changing in time, is ρ_{ij}. As a preprocessing step, the time average at each gridpoint, as well as the average over all gridpoints at each time step, is subtracted from the data, yielding a matrix $\overline{\boldsymbol{P}}$ with elements given as:

$$\overline{\rho}_{ij} = \rho_{ij} - \{\rho_i\} - \{\rho_j\} \tag{1}$$

where $\{\rho_i\}$ and $\{\rho_j\}$ are given by:

$$\{\rho_i\} = \frac{1}{J}\sum_{j=1}^{J} \rho_{ij} \quad \{\rho_j\} = \frac{1}{I}\sum_{i=1}^{I} \rho_{ij} \quad , \quad i,j = 1,2,3\ldots I,J. \tag{2}$$

Next, the elements of the covariance matrix, $\boldsymbol{C}$, are determined by

$$c_{i,k} = \frac{1}{J}\sum_{j=1}^{J} \overline{\rho}_{ij}\overline{\rho}_{kj} \quad i,k = 1,2,3\ldots I \quad , \quad j = 1,2,3\ldots,J. \tag{3}$$

The symmetric covariance matrix is of dimension $I\times I$ as usually $I\times J$. $\boldsymbol{C}$ captures the correlation among the columns of the original data matrix, indicating to what extent the temporal evolution of the variance in a given grid point is related to others. Using eigenvalue decomposition, the eigenvalues λ, and eigenvectors, ϕ, of $\boldsymbol{C}$ can be found:

$$\boldsymbol{C}\phi_i = \lambda_i\phi_i. \tag{4}$$

The first eigenvector direction (first mode) corresponds to the largest eigenvalue, capturing the direction along which the variance in matrix $\overline{\boldsymbol{P}}$ is maximal. The first few modes (we order by decreasing eigenvalues) explain the primary dynamics of a system. As all eigenvectors are pairwise orthogonal, each mode represents an independent property of the system.

By computing the temporal amplitude of each mode, the timescale of the corresponding processes can be obtained. The amplitude of the ith mode is found by projecting the density deviation matrix $\overline{\boldsymbol{P}}$ onto the ith spatial eigenvector direction:

$$A_i = \overline{\boldsymbol{P}}\phi_i. \tag{5}$$

The original matrix of data can be reconstructed by summing the products of the amplitudes and spatial eigenvectors for all I modes:

$$\overline{\boldsymbol{P}} = \sum_{i=1}^{I} A_i\phi_i. \tag{6}$$

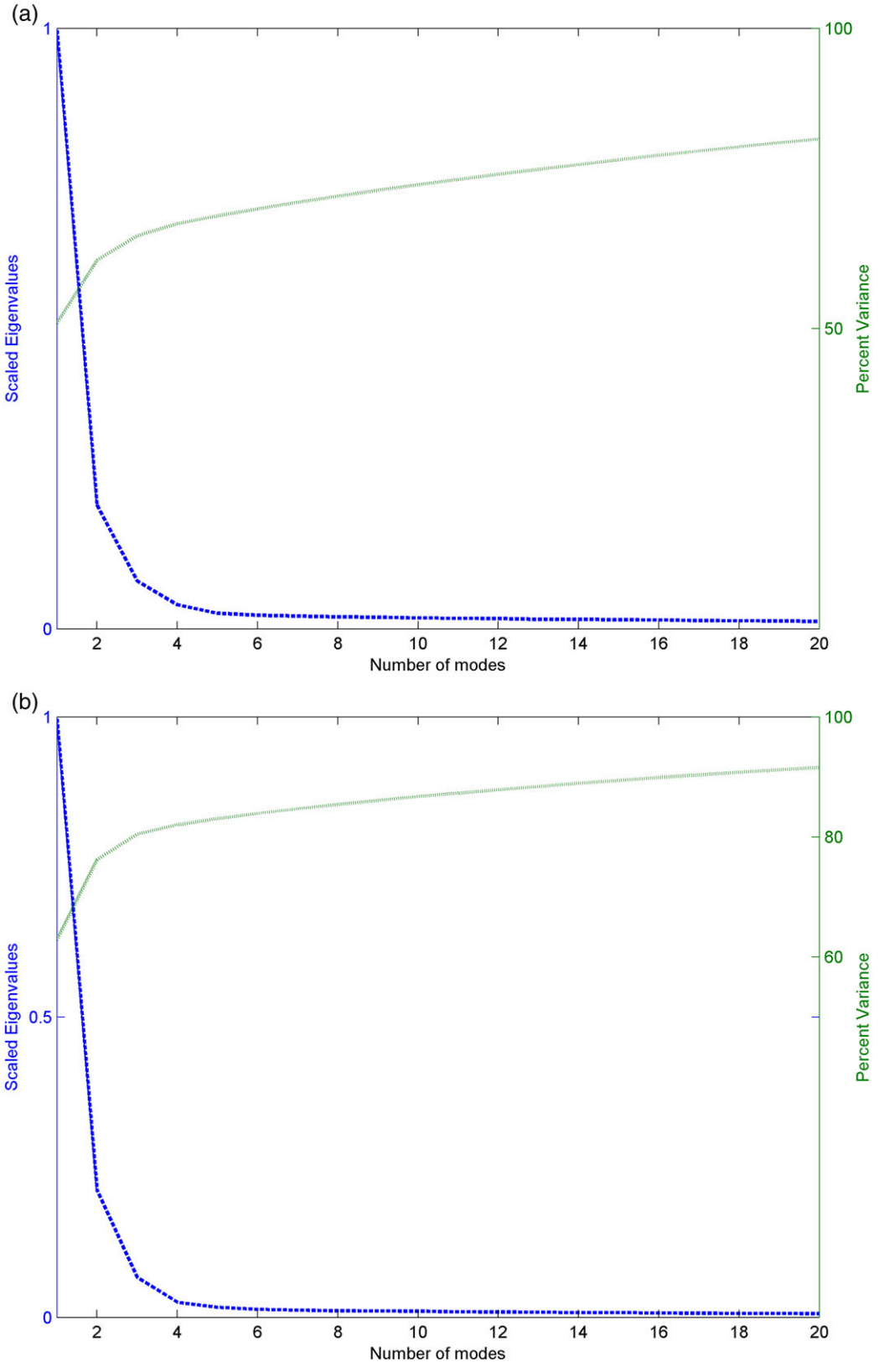

Fig. 3. Scree plots of DLPC (a) DSPC (b).

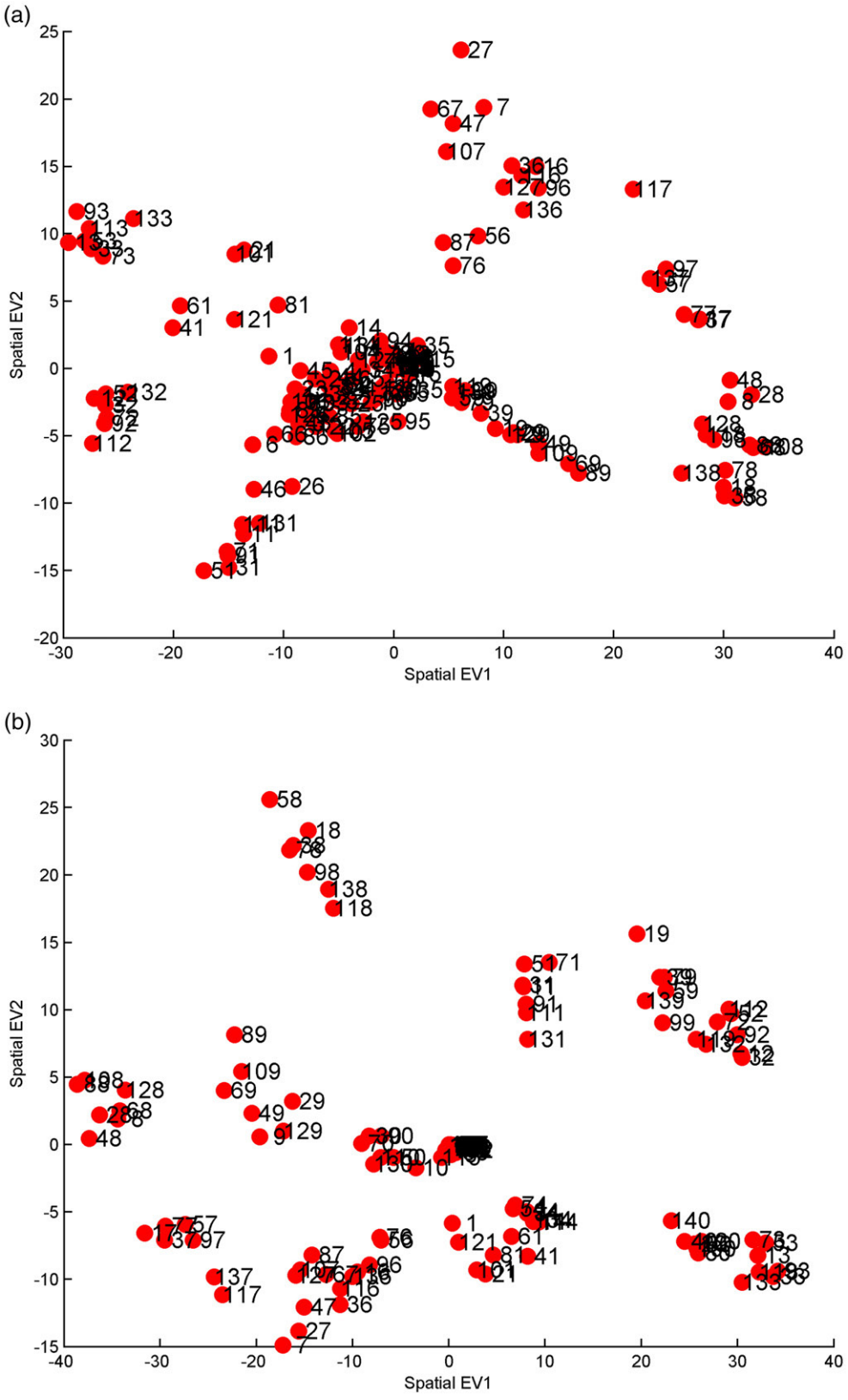

Fig. 4. Plotting the first and second spatial eigenvectors against each other for (a) DLPC and (b) DSPC.

If a small number of modes, $N \ll I$, are selected judiciously to represent the majority of the variance in the dataset, the residual space contains only random features, i.e. noise:

$$\boldsymbol{R} = \sum_{i=1}^{I} A_i \Omega_i - \sum_{i=1}^{N} A_i \Omega_i. \tag{7}$$

The residual matrix $\boldsymbol{R}$ visualizes the data not described by the inclusion of N modes. The amount of variance captured by the inclusion of N modes can be quantified using the percent cumulative variance:

$$\%\mathrm{CV} = \frac{\sum_{i=1}^{N} \lambda_i}{\sum_{i=1}^{I} \lambda_i} \times 100. \tag{8}$$

At this point, a comment on the selection of the number of grids chosen for KLE in the bilayer system is in order. This number should be chosen to ensure that the lower-dimensional model captures the relevant dynamical features of the system. If there are too many gridpoints, the number densities will only be single occupancies or unoccupied grids which will bias the KLE by destroying the definition of a continuous density leading to focus only on the local dynamics of the system. If there are too few grids, phase behavior and local actions will be difficult to observe and the analysis will be limited to global changes. Our experience has been that as long as the number of grids is chosen reasonably, the impact of gridsizing on KLE performance is minimal [26].

3. Results and discussion

For four different simulations of DLPC and DSPC mixtures in bilayer leaflets, KLE was applied to the two-dimensional density distributions to elucidate membrane features contributing most to changes in density structures. To validate the results and to provide a basis for interpreting the characteristics of the primary modes, it is necessary to have an understanding of trends in the raw physical data. (To visualize changes in phase patterns and bilayer shape over time, movies which show the position of headgroups in the bilayer over time were recorded for each system. These are available at http://www.chms.ucdavis.edu/web/research/faller/KLmovies.html). This section will analyze the properties of each system as it evolves in time and discuss the results of the KLE of each layer in order.

3.1. Domain instability due to temperature

The first system is simulated at a (unphysically high) temperature of 385 K, which is high enough to melt any gel phase and reduce changes in the system to random diffusion in a well-mixed fluid phase [16,34]. The system was set up in a structure with gel-phase DSPC and liquid-phase DLPC in a stripe-wise arrangement. The pieces of gel and liquid bilayers or monolayers had been equilibrated earlier and the simulations were then patched together [27]. Both leaflets have equal concentrations of 328 DSPC and 528 DLPC molecules. Fig. 2 shows the headgroup positions in a side-view. From these snapshots of the system several observations can be made. The initial state of the bilayer (Fig. 2a) was constructed by simply distancing the headgroups across the center of the membrane according to the amount of space that the apolar tailgroups occupy. The transbilayer distances between DSPC molecules are larger than that for DLPC lipids. The initial state is characterized by sharp edges at the interface between regions of DSPC and DLPC, a characteristic that does not appear to be stable. In the second time step (after 1 ns), the bilayer and simulation box contract in all directions and undulate (Fig. 2b). As we only analyze the two-dimensional projection of the density this undulation may lead to some coupling of eigenvectors which we, however, neglect in the following. The undulated state appears to be more stable than the initial. The sharp edges have smoothed to form a more continuous contour. The locations of interfaces between DSPC and DLPC have not been shifted appreciably. Over the course of the simulation, the bilayer begins to lose order (Fig. 2c). For this system, an 8×20 grid was used to make gridspaces approximately square, as the system itself was not square. Each grid contains on average 3.3 DLPC and 2.1 DSPC.

A Scree plot shows the amount of variance captured by a given number of modes, as it increases with the number of modes and allows the selection of a suitable low-dimensional space for the representation of the data. Fig. 3 compares the results for one of

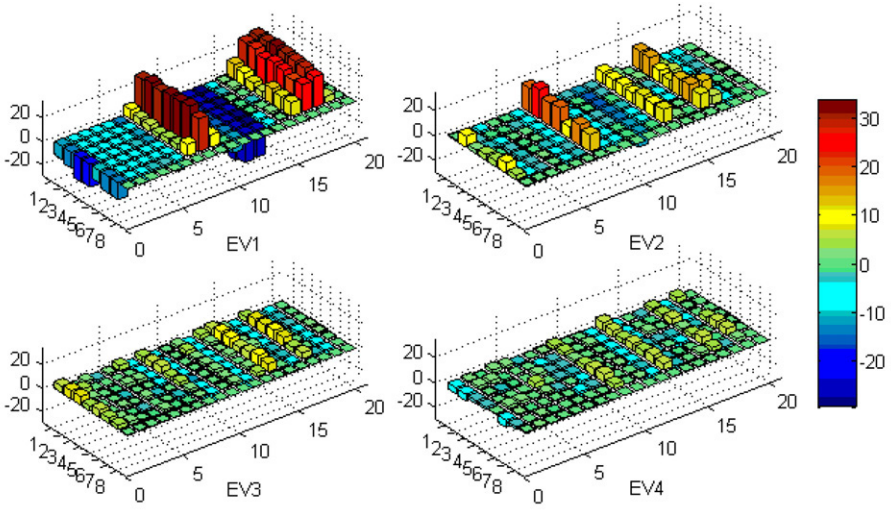

Fig. 5. Components of eigenvectors for the first four modes of DLPC on bottom layer.

the leaflets for each species. The amount of variance explained by the first few modes for DSPC is larger than that for DLPC. The inclusion of four modes explains about 67% of the data for DLPC and 82% for DSPC. One possible explanation for this result is that DLPC is smaller than DSPC and correspondingly more mobile. Furthermore, DSPC prefers the gel phase more than DLPC and it

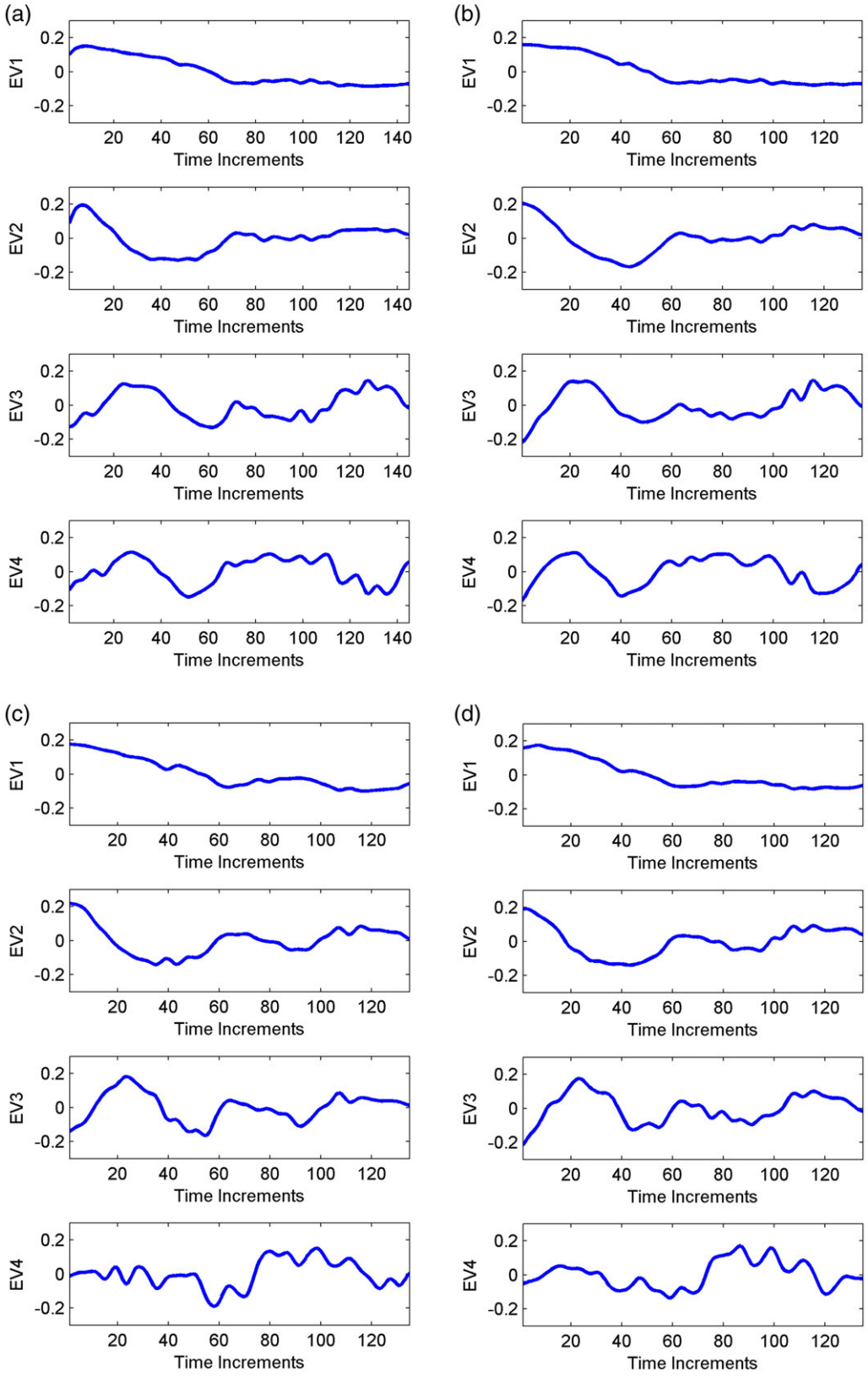

Fig. 6. Temporal amplitudes of the first four modes for 1st bilayer system.

is possible that there is a more structured movement of DSPC as opposed to simple diffusion.

Spatial eigenvectors indicate how the corresponding mode is distributed in the bilayer. If the first two spatial eigenvectors are plotted against each other (Fig. 4), specific grid positions cluster indicating a coherent motion. For both lipid species, it appears that the cluster members are separated by 20 gridspaces. Since the gridding for the bilayer is 20 spaces long and 8 spaces wide, this indicates that the groupings represent a set of values oriented horizontally along the simulation box. This essentially means that

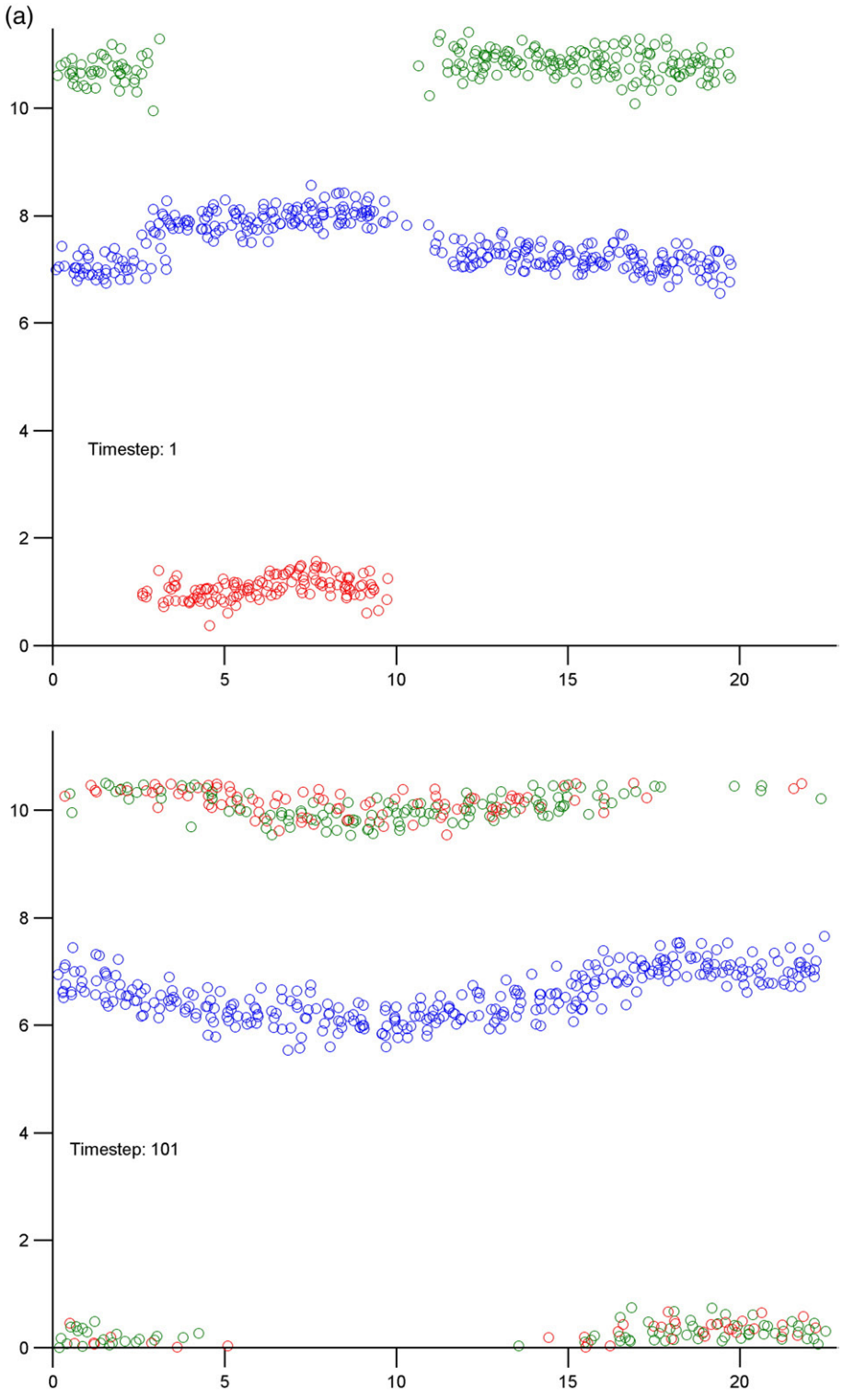

Fig. 7. Initial and final bilayer side-views (a), and initial three-dimensional view (b).

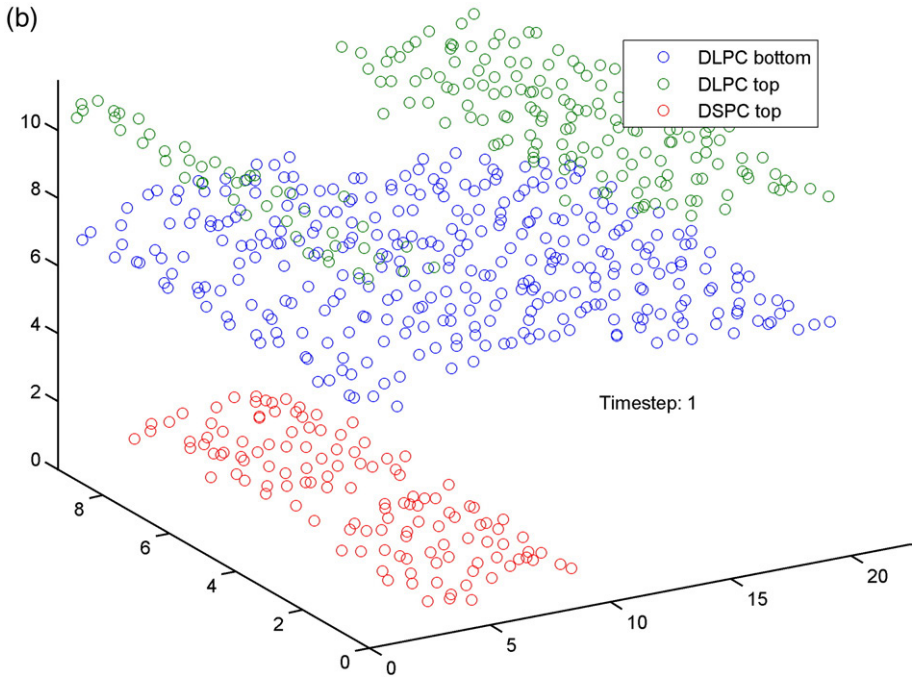

Fig. 7 (*continued*).

gridspaces have similar magnitude in the horizontal direction for both the first and second mode. This is understandable as the phase stripes shown in Fig. 2 are infinitely long. Greater deviations in lipid density are anticipated in the direction perpendicular to phase boundaries due to inter-phase movements. The components of the modes for DSPC are more organized than for DLPC. This again hints that DSPC diffuses more uniformly than DLPC. We also observe that the first and the second modes are complementary between DSPC and DLPC indicating that inter-phase diffusion is present.

Fig. 5 plots the components of the spatial eigenvectors for the first four modes of DLPC along the grid of one leaflet. The shape and distribution of the first spatial eigenvector indicates that the main contribution comes from DSPC sites located near the interface and largely indicates the density gradient between phases that is responsible for the bending motion. As the bilayer loses order, the simulation box expands resulting in the migration of the interfaces. The greatest changes in density are expected from the movement of interfaces into gridspaces that were formerly unoccupied. Recall that we operate on a fixed and not a scalable grid. The alternating positive and negative peaks can be explained by the lipids entering a gridspace due to expansion closely followed by the exit of a group of lipids in another. The second spatial eigenvector appears to explain the regions of highest concentration as opposed to the interfaces between species. The 3rd and the 4th eigenvectors show rather insignificant characteristics compared to the first two and capture more local dynamics.

For this system, the gel-phase region eventually disappears and we observe a liquid phase with free diffusion. However, the system does not completely mix in the course of the simulation. The first mode represents the initial global change associated with a bending motion and the subsequent modes provide more localized corrections to the first mode. This is corroborated when the temporal amplitudes of the spatial eigenvectors are considered (Fig. 6). The temporal behaviors of the first three modes for each category of lipids mirror each other very closely. This demonstrates that the main processes that alter the bilayer structure are closely related across species and leaflets. Only in the fourth mode are there any noticeable differences. Here, the two layers undergo different processes in the beginning but afterwards a commonality among the amplitudes is observed which becomes active at about 50 time steps in one layer and about 80 time steps in the other. The first mode in each instance is initially active and spans the first 60 time steps decaying exponentially. This motion suggests global change as well as a major long term shift in the system towards equilibrium. The second mode is also initially active but shows a faster dynamics than the first. With increasing number of modes, the amplitudes become more oscillatory (and their influence wanes as shown in Fig. 5), indicating local random dynamics.

This bilayer domain structure exhibits immediate deformation due to non-equilibrium initial conditions. It leads to an undulation motion that relaxes back to the equilibrium state which is close to the initial state. The dominant motion is associated with the bending mode and not much mixing is observed between the lipids. The intra-bilayer motion is weaker than the bilayer undulation. The separation between lipids is stable but the interface is unstable. The first mode captures about 55% of the variance. The second mode is weaker (it adds about 10% variance) and is associated with the local arrangement of lipids at the interface. The second spatial eigenvector shows contribution from sites near the interface but mostly from within the DLPC sites. We conclude that the first mode captures the

physical motion of the bilayer while the second mode captures the motion of the lipids. Higher modes capture local diffusion and do not show relevant structure. The bending mode takes about 80 time steps (80 ns) and decays exponentially. The rearrangement of lipids at the interface is faster and as the lipids orient along the interface, they overshoot their final rearrangement

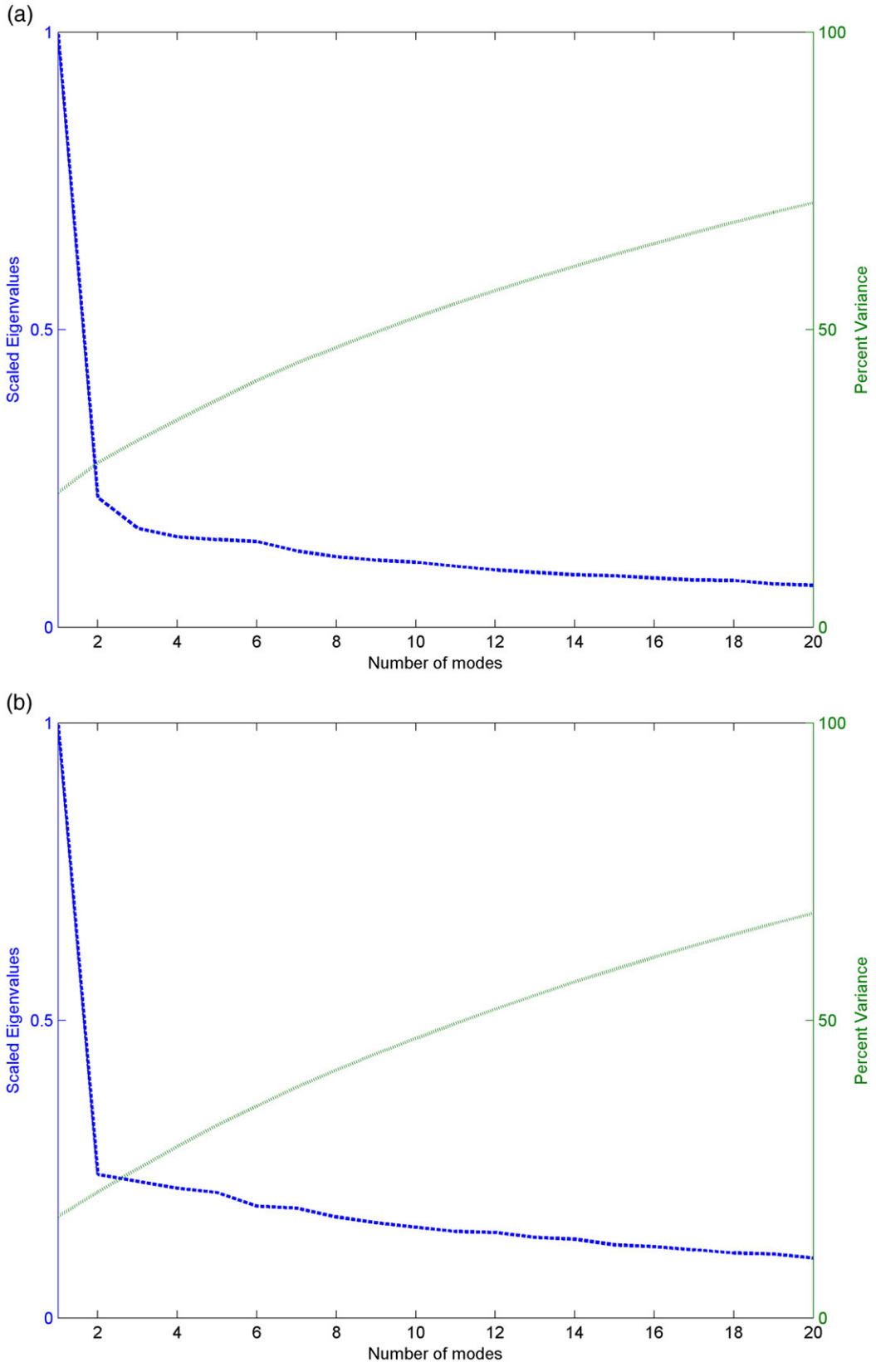

Fig. 8. Scree plots of DSPC (a) and DLPC (b) on top layer.

due to the slower motion of the interface. The modes indicate largely block motion of the phases, ruling out mixing and confirming a cohesive global rearrangement that dominates the dynamics.

3.2. Domain instability due to uneven lipid distribution

In the second system, the two leaflets contain unequal amounts of each lipid as real cells have tightly controlled concentrations in the two leaflets. The simulation is run at 295 K. Fig. 7 shows that only one layer contains DSPC. In this example, 328 lipids are on each layer with one containing 128 of DSPC and 200 DLPC. The gridding is chosen as 12×6. Considering the Scree plots in Fig. 8 compared to Fig. 3 above, we note that the first two modes capture less of the variance for both lipids (about 30%). Instead of a smooth exponential decay of the scaled eigenvalues, we observe a discontinuity after the second mode, and the higher modes have almost equal contributions to explain the overall variance. With less variance captured by the primary modes, it can be concluded that the motion is less structured. Compared to the first system, the bilayer dynamics are more dominated by diffusion and less by the transition from one state to another. As the original structure breaks down, DSPC enters the surrounding phase. This results in a gradual decrease in the concentration in the areas DSPC originally inhabited and an increase in others. A consideration of the first four spatial eigenvectors in Fig. 9 supports this observation further. We still observe peaks at the interfaces between lipid species. However, there are no points where the components of the first mode are close to zero. The first spatial eigenvector shows positive regions where DSPC resides initially and is negative at all other gridspaces.

The initial structure is characterized by sharp lateral distances between phases but after the first time step, an adjustment corrects for this and the contour of the bilayer smoothes across boundaries. In the final state, the original structure breaks down completely, and the two lipids are mixed (Fig. 7). Over the course of the simulation, the bilayer shrinks in width and expands in length. The thickness of the bilayer becomes more uniform as it loses order and the DSPC lipids stratify across the membrane. This implies that the first mode is dominated by the expansion of the system. The other modes appear to be fairly random indicating that local diffusion is as important as the expansion of the phases. Although at a lower temperature than before, this bilayer system is unstable due to the uneven concentration of lipids in the leaflets. It appears that DSPC domains in one leaflet are more stable if they are coupled to another gel-domain on the other side in agreement with experiments [29]. Fig. 10 plots the first spatial eigenvector against the second. We see fewer groupings than in Fig. 4 above. Some horizontal orientation is observable but, in general, this plot is much less organized and lacks any meaningful spatial correlation, supporting the mixing mechanism.

Fig. 11 shows the temporal amplitude of the first four modes for all species in the bilayer system. For the first mode, all three categories of lipids show similarity in their activity. Initially, the first mode becomes active but decays after about 60 time steps. DLPC amplitudes on the bottom layer are similar to the top layer, indicating the motions of the two layers are correlated. This similarity in the first mode indicates that the layers share this common dynamic feature, the expansion of the phases. It can also be seen that for DLPC, the second mode evolves similarly.

3.3. Domain instability due to undulations in the bilayer

The third example is a bilayer with an extreme initial undulation and a small patch of DSPC in both layers. It is composed of 800 DLPC and 100 DSPC lipids on both sides. Fig. 12a shows the placement of the lipids in the first time step. It can be seen here that as the initial highly undulated structure breaks down with time, it transforms into two parallel leaflets. After 914 time steps (731 ns), the DSPC (shown in cyan and red), which was limited to a distinct region initially, becomes more stratified across the

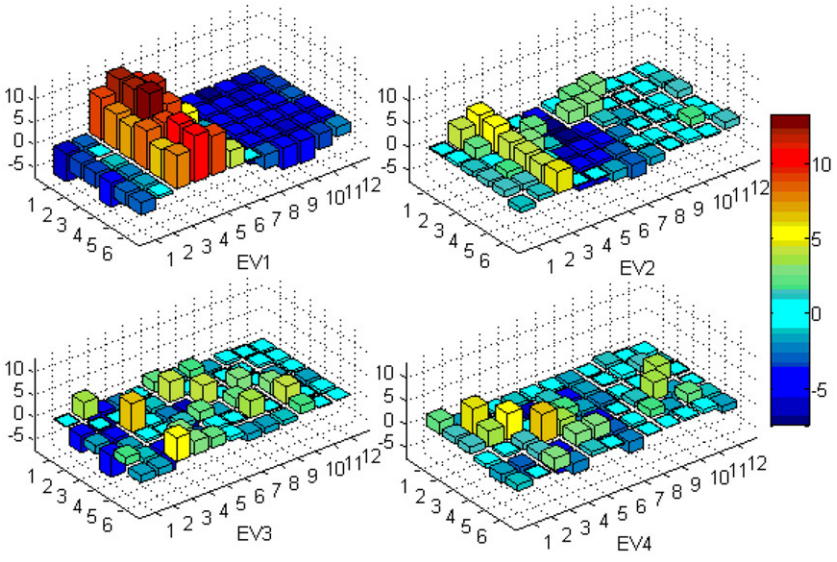

Fig. 9. Component plots of the first four modes for DSPC on top layer.

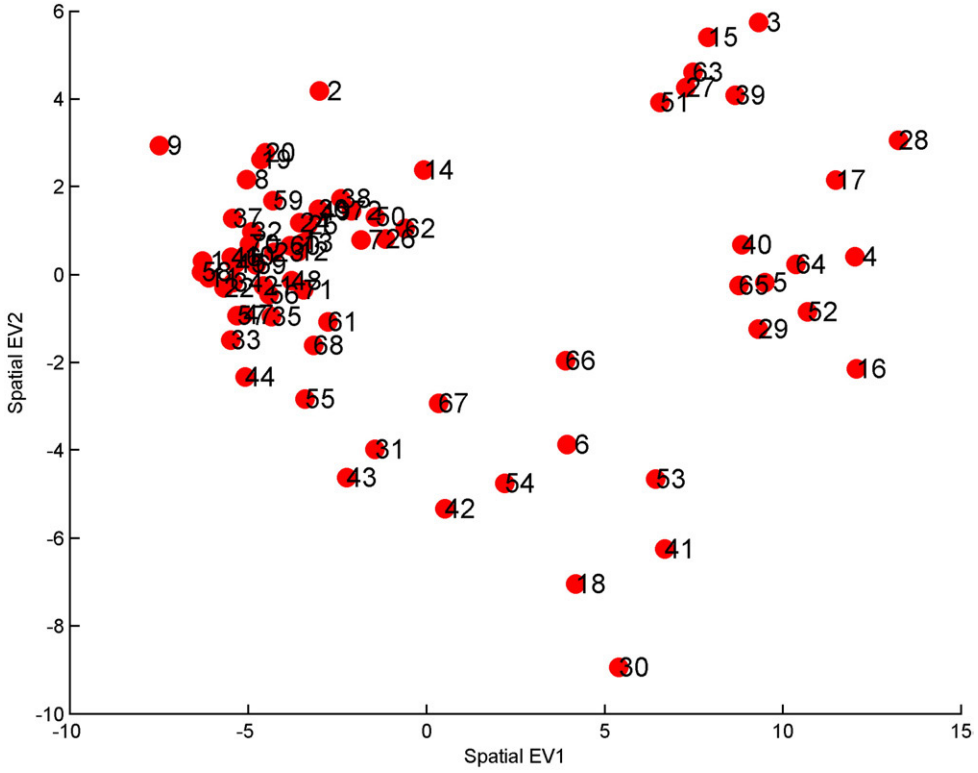

Fig. 10. Comparing eigenvector components of the first two modes for DSPC on top layer.

membrane. As DLPC diffuses into DSPC, the average tail length of the region DSPC occupies decreases slowly whereas in other regions it increases. As the tail lengths in each gridspace average out, this creates a driving force towards the flattening of the bilayer system. This also results in a more uniform distance between bilayer leaflets which can be seen in Fig. 12. Diffusion is somewhat inhibited by membrane undulations as there is more opportunity for steric hindrance at the crests and troughs of the contour. Fig. 13 shows the Scree plots using a 10×10 grid. Contrary to the first case, few modes are needed to capture the variance of the dynamics of DLPC than of DSPC. The most significant dimensionality reduction occurs with DLPC in the bottom layer where just four modes explain about 80% of the variance in the data. The first two modes of DLPC capture about 60% and 10% (total 70%) variance, respectively. DSPC on the other hand has 50% and 5% (total 55%) variance. The second mode for DSPC clearly has less influence than the one for DLPC and for both, higher modes have almost equal weight in explaining the variance. This is perhaps expected since the influence of random diffusion and noise is more attenuated for DSPC due to its larger size.

Again considering the spatial eigenvectors in Fig. 14 for the first four modes, one observes that the area of greatest change appears to be not at the interface between DSPC and DLPC but at the edge of the undulation which can be explained by the large change in projected density. Because of the undulation, gridding based on pure *xy* position becomes somewhat problematic as the density in the layer is biased by the shape of the bilayer contour. The second mode marks a place where the greatest region of concentration occurs in the bottom layer. The third and fourth modes describe largely uninteresting local dynamics. We have seen that the bilayer essentially expands over time whereby the position of the peak of the undulation changes. The first four modes show an incomplete coupling between leaflets. We see that DSPC in the bottom leaflet behaves differently than the other three groups which are coupled. It becomes clear why the Scree plots show more variance captured for DLPC than for DSPC with smaller number of modes as the eigenvector plots for DLPC contain more structure. Higher modes for DLPC (not shown) merely contain corrections to the first mode. In the top layer, there is a net loss of lipids from the regions they occupy at the beginning of the simulation as they travel into gridspaces on the right hand side of the bilayer. Note here the larger number of lipids diffusing to the right. This is likely because of the hindrance to movement presented by the undulation. In the bottom layer, we can see that there is some minor movement to the right but, compared to the top layer, there is significantly more inward movement between the two peaks as well as movement to the left.

The first spatial eigenvectors for each species on the top and bottom layers are plotted on the grid in Fig. 15. For DLPC, a strong similarity can be seen in both layers. The first mode is dominated by the expansion of the bilayer. As additional gridspaces become occupied, the KLE detects a strong change in density in these regions. There are also small peaks in these plots in the areas that DSPC initially occupies indicating that DLPC has diffused into these regions. There are strong negative regions in the two plots for DLPC towards the left side of the bilayer.

Fig. 16 shows the evolving temporal amplitudes of the first four modes for each species. All of the amplitude plots indicate

that there are common mechanisms of change associated with both species in each layer. The only mode that seems to differ significantly is the fourth mode for DSPC on the top layer. The first mode shows a long term global process changing sign midway through the simulation. The time scale of the process is shorter for DSPC than for DLPC.

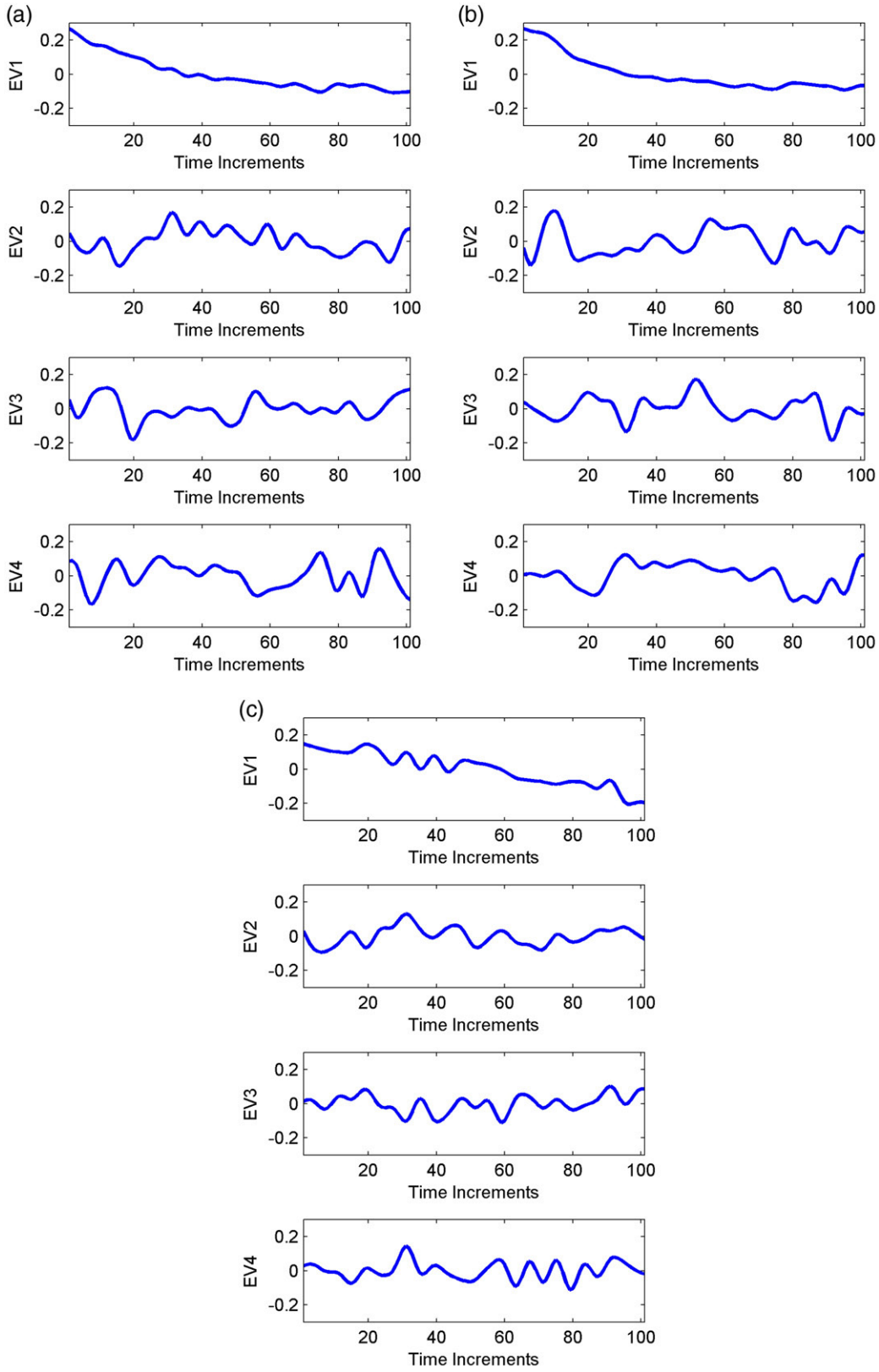

Fig. 11. Temporal amplitudes of the first few modes for all species in 2nd bilayer.

3.4. A stable bilayer system for comparison

The stability of a system is often difficult to characterize. The classical understanding of a stable system is one which does not change but fluctuates around a stable equilibrium. The fourth and last system in this study is the most stable system. There is a lack of global change and subsequently the KLE results are limited to local dynamics. Fig. 17 shows a side-view of this bilayer. One layer is shown in blue and red and the other in cyan and green. Both leaflets are in phase the thickness modulation is caused by

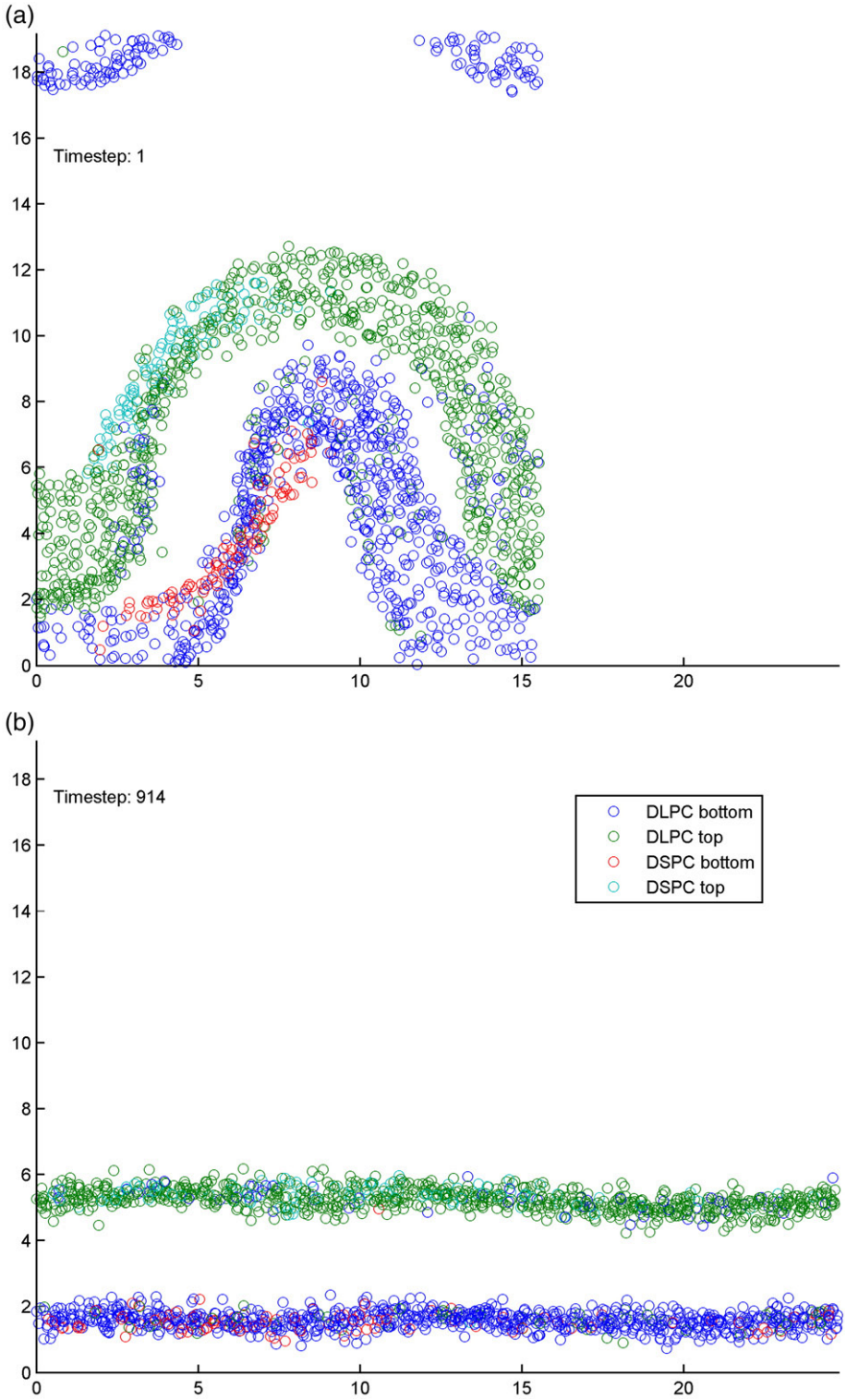

Fig. 12. Initial and final contour plots for the 3rd bilayer system (side-view).

the different lipid lengths. Due to periodic boundary conditions it only appears as if DLPC leads to a larger thickness. Each leaflet contains 150 DLPC and 100 DSPC. In the first time step, the DSPC is arranged into a stripe surrounded by DLPC. The two nearly parallel layers have regions of DSPC and DLPC directly on top of each other, creating a larger transbilayer distance between

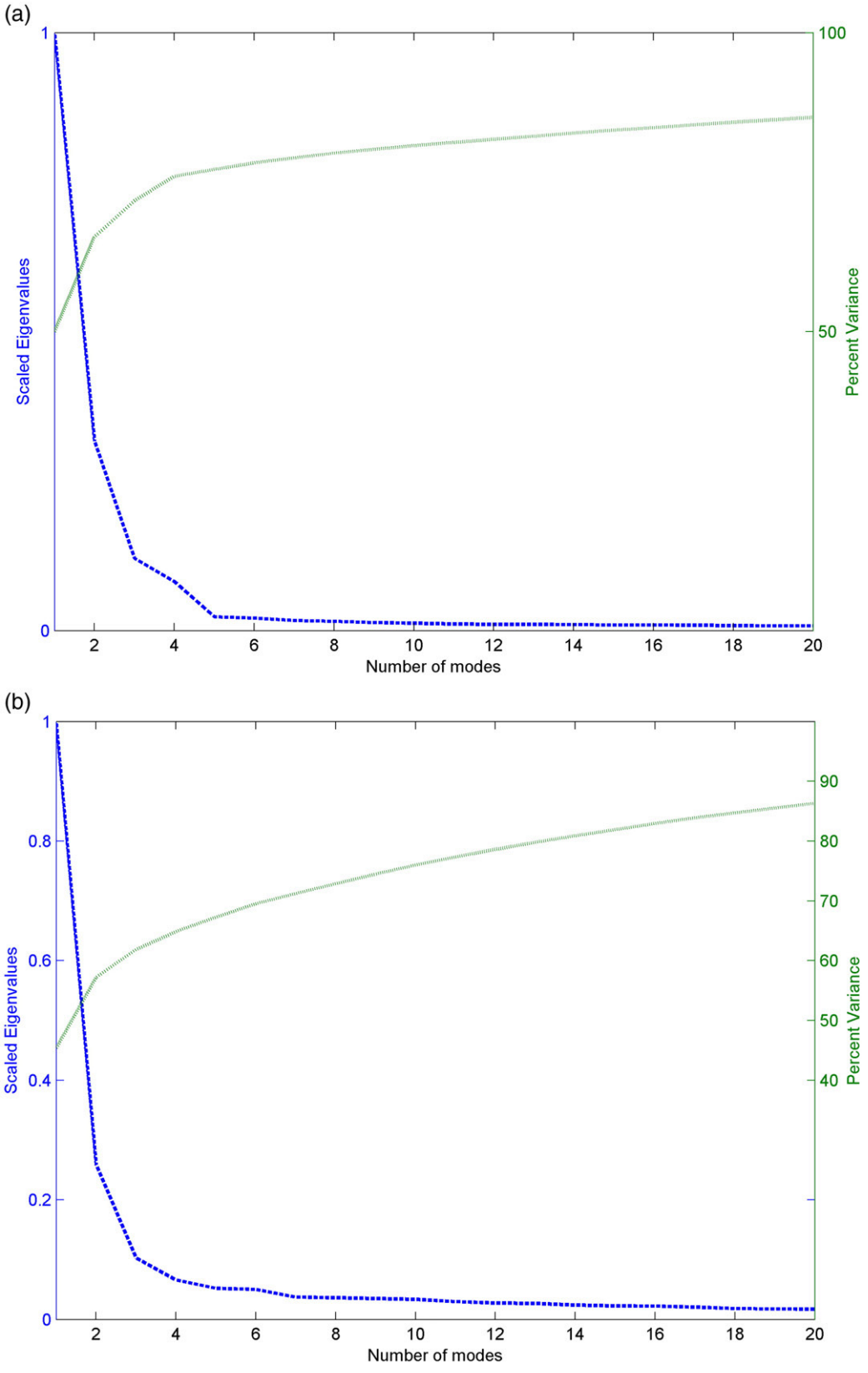

Fig. 13. Scree plots for the 3rd bilayer system.

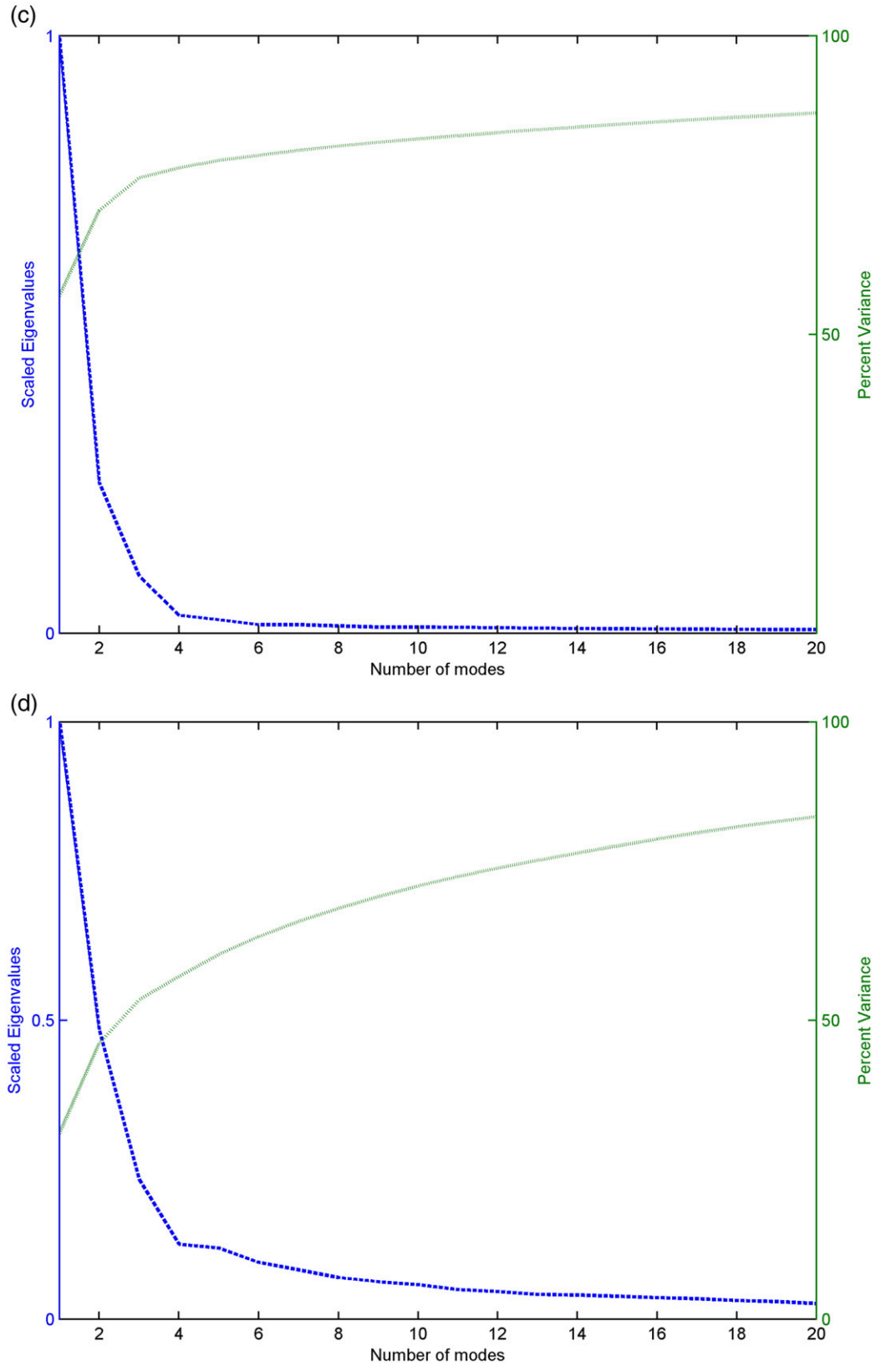

Fig. 13 (*continued*).

the two DSPC phases. The final time step in Fig. 17b does not show significant differences. The contours of both layer membranes have only marginally changed and a few DSPC lipids in each leaflet have diffused to the right side of the bilayer. The simulation box has expanded negligibly. This is a stable system, and no structural deformation is observed.

The modes indicate diffusive behavior and contribute almost equally to the variance. The spatial eigenvectors show some local structure. Fig. 18 shows the Scree plots for DSPC and DLPC in one layer. The magnitudes decay weakly with increasing mode number and there is no separation into dominant and lesser. The cumulative variance curves are nearly linear and the first mode in both cases represents less than 10% of the variance. The first 20 modes explain only about 45% of the variance for DLPC and 60% for DSPC. A perfectly random system would have eigenvalues which, when plotted as a histogram according to their magnitude, would conform to a Gaussian distribution. Fig. 19 shows a histogram plot for the percent variance explained by each mode individually for both species. This system lacks global changes that dominate the motions of lipids. Each mode represents a small

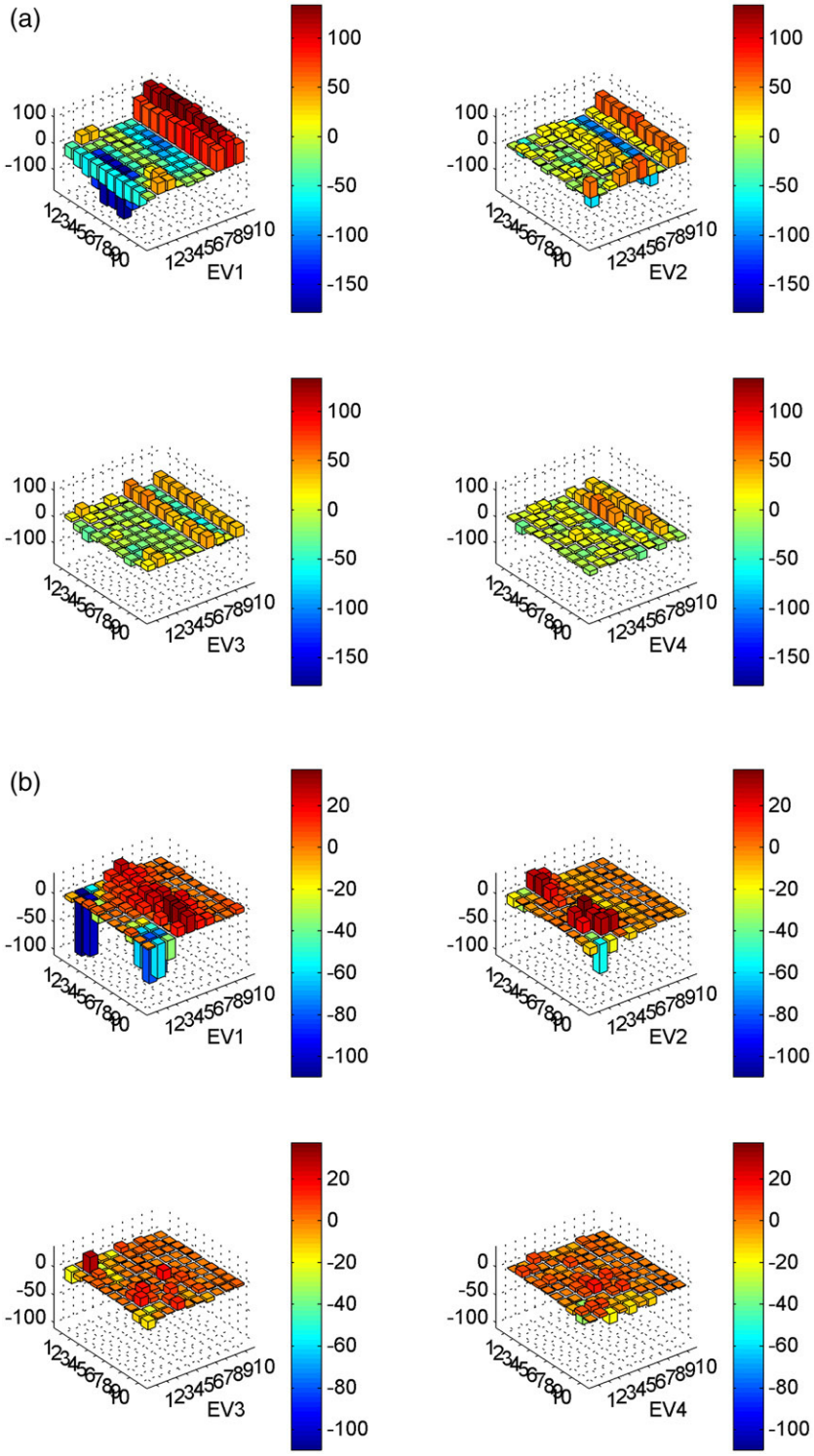

Fig. 14. Spatial eigenvectors for both lipids in both layers, DSPC left, and DLPC right.

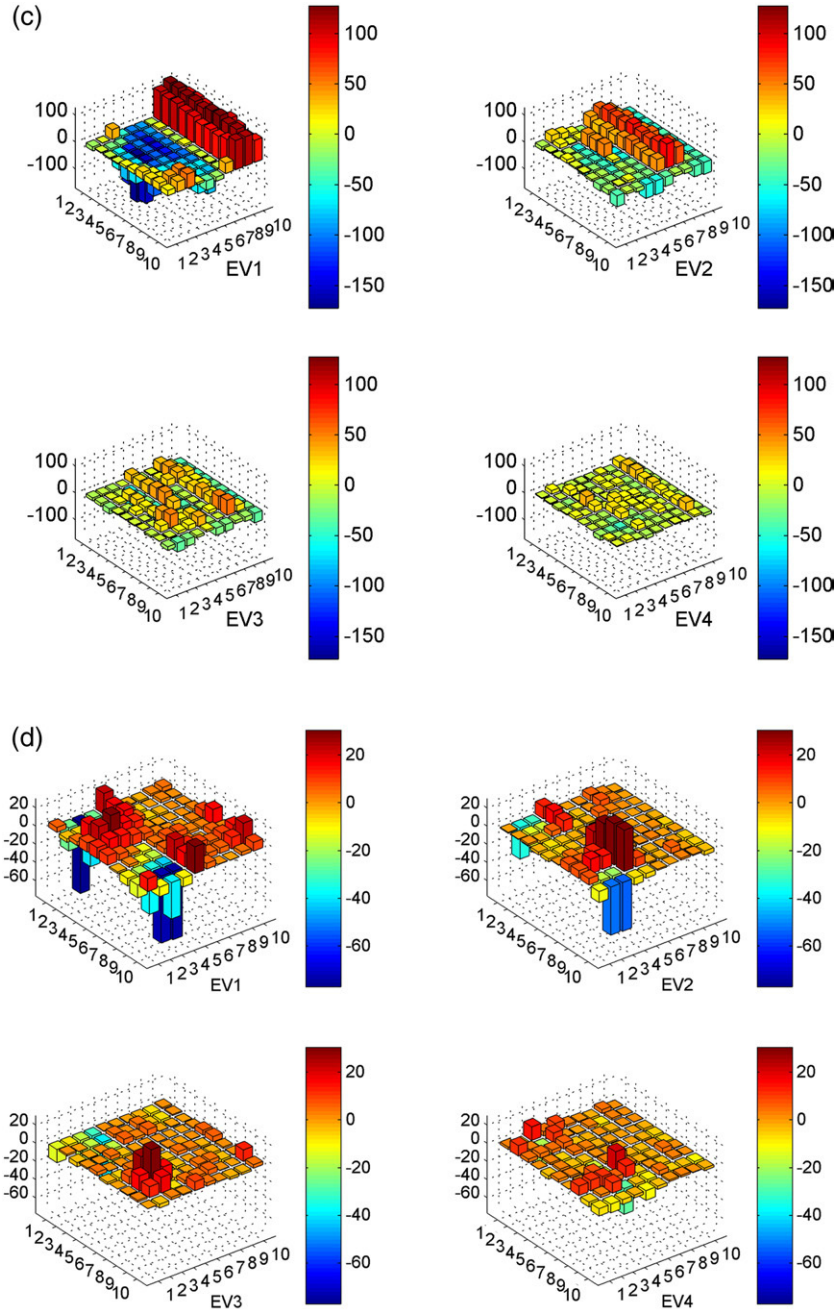

Fig. 14 (*continued*).

adjustment from the original structure. DSPC is better described than DLPC with a given number of modes. The spatial eigenvectors appear to be complementary between DLPC and DSPC. Fig. 20 shows the first four modes for DLPC which share equal importance to changes in the density distribution matrix. In the eigenvector component plots for DLPC, regions occupied by DSPC have components which are at or near zero, and vice versa. This indicates that DLPC and DSPC prefer to migrate within their respective phases as opposed to separating from the phase structure. The majority of the components take on their greatest value within their own phases. This means that the greatest changes that occur in the system are due to density changes within each phase. The first two modes focus on the dynamics closer to the interfaces between DSPC and DLPC. Fig. 21 shows that the temporal amplitudes are small and are largely correlated between lipids on the same layer. In this case, the movement of each monolayer is independent of one another.

4. Conclusions

We have demonstrated that KLE is a powerful tool for unveiling the primary mechanisms of phase decomposition in a lipid bilayer system and to characterize its stability. By creating a set of eigenvectors, unique actions that contribute to changes

in the density distribution matrix are revealed as eigenvectors are orthogonal. The analysis pinpoints the locations of interest in the bilayer and describes each mode with its importance over time. Yet the expansion can only abstractly describe the modes of change and does not identify its physical significance. It is necessary to analyze the raw data in conjunction with performing the expansion to make sense of its results. So a combined approach is suggested as standard analysis without KLE may miss

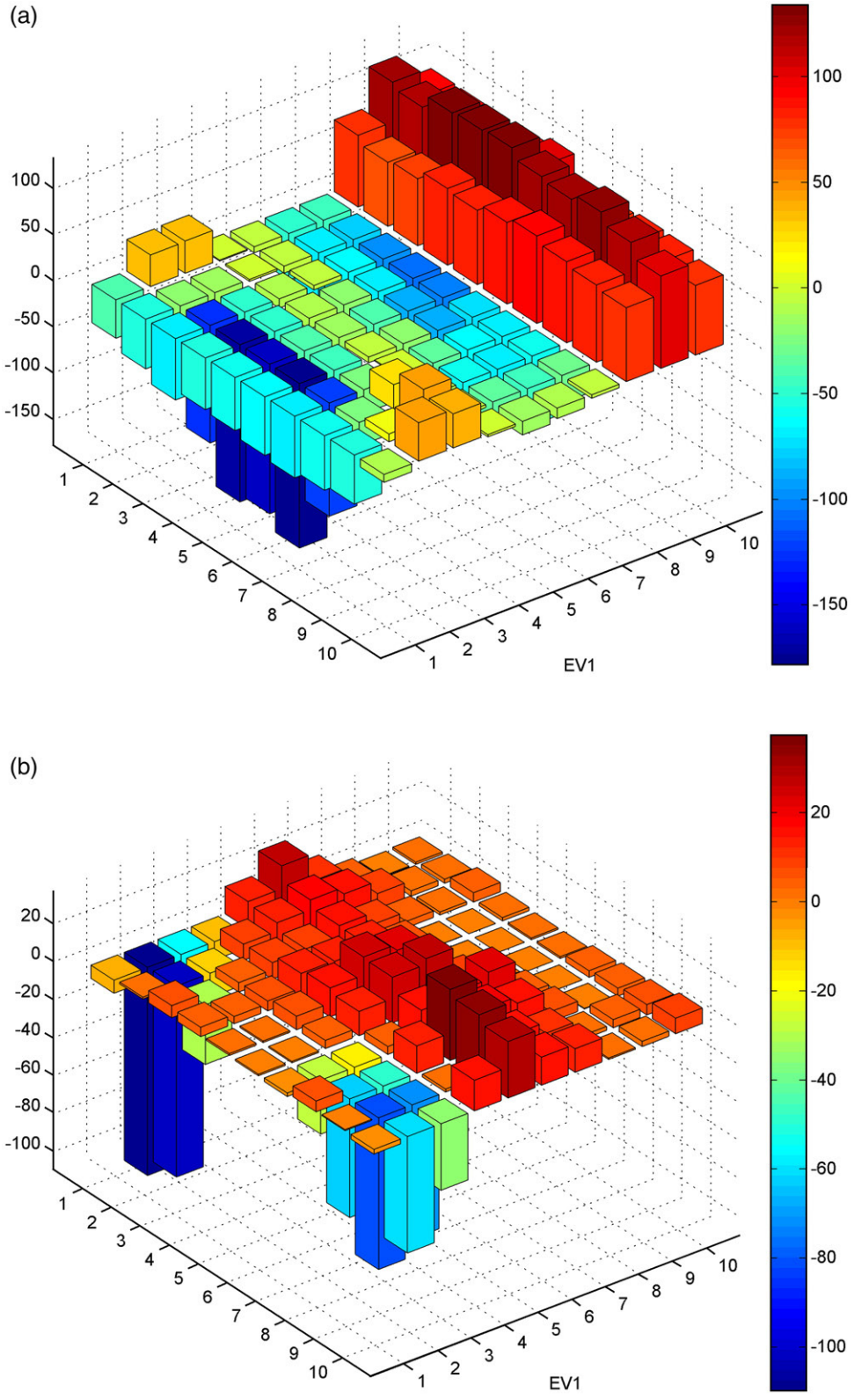

Fig. 15. Components of spatial eigenvectors for the first mode in all species.

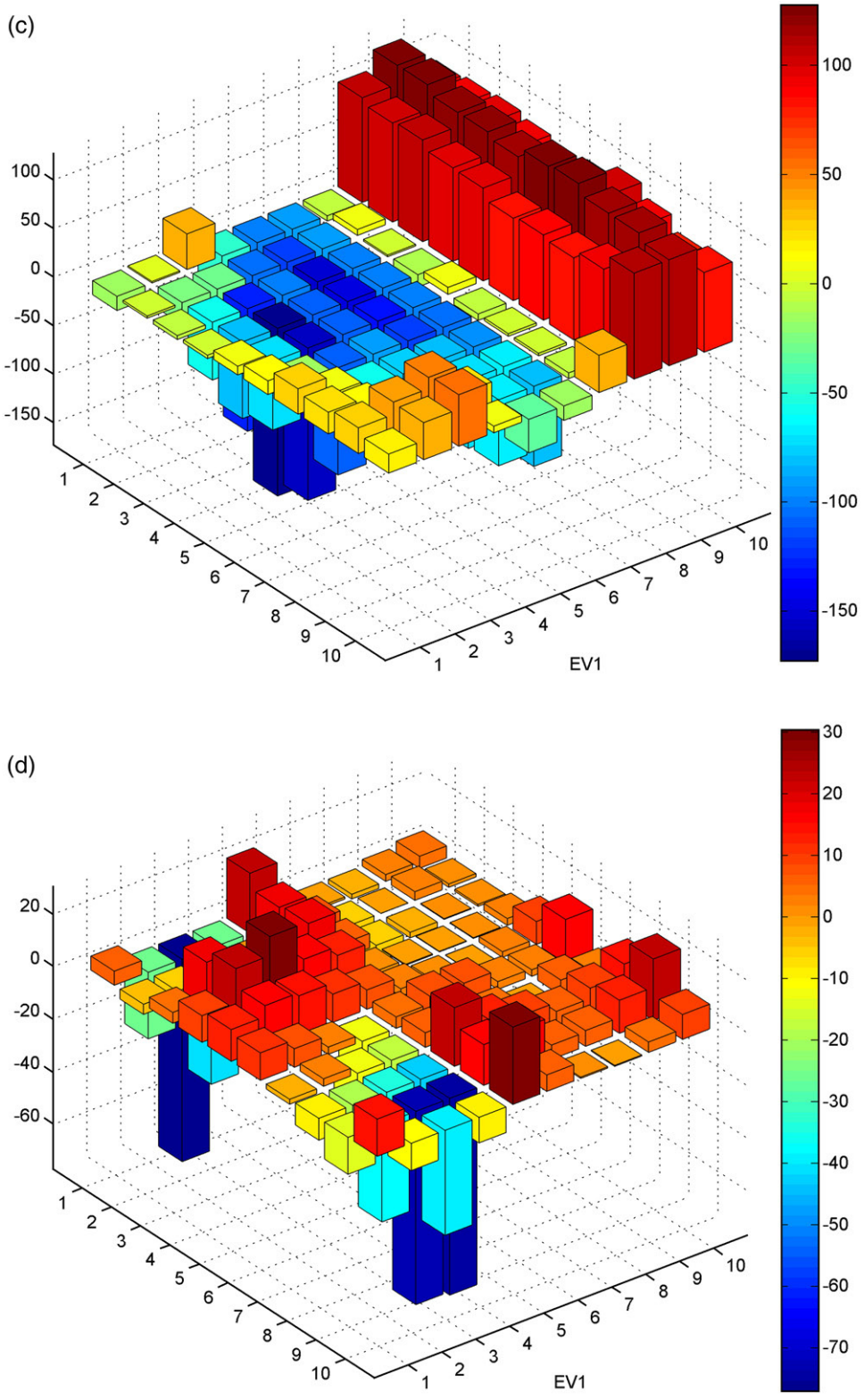

Fig. 15 (*continued*).

large scale correlated motions. On the other hand, an abstract analysis of the modes might produce superfluous conclusions disassociated from their physical meaning.

Let us summarize the main findings in our systems: In all cases, DSPC showed a more structured motion than DLPC which correlates with DLPC preferring the fluid phase and having faster dynamics [16,34]. We find that the first mode for each simulation corresponded to a long term global process and subsequent modes present corrections to the global dynamics. In the 2nd system compared with the first, we found that not only

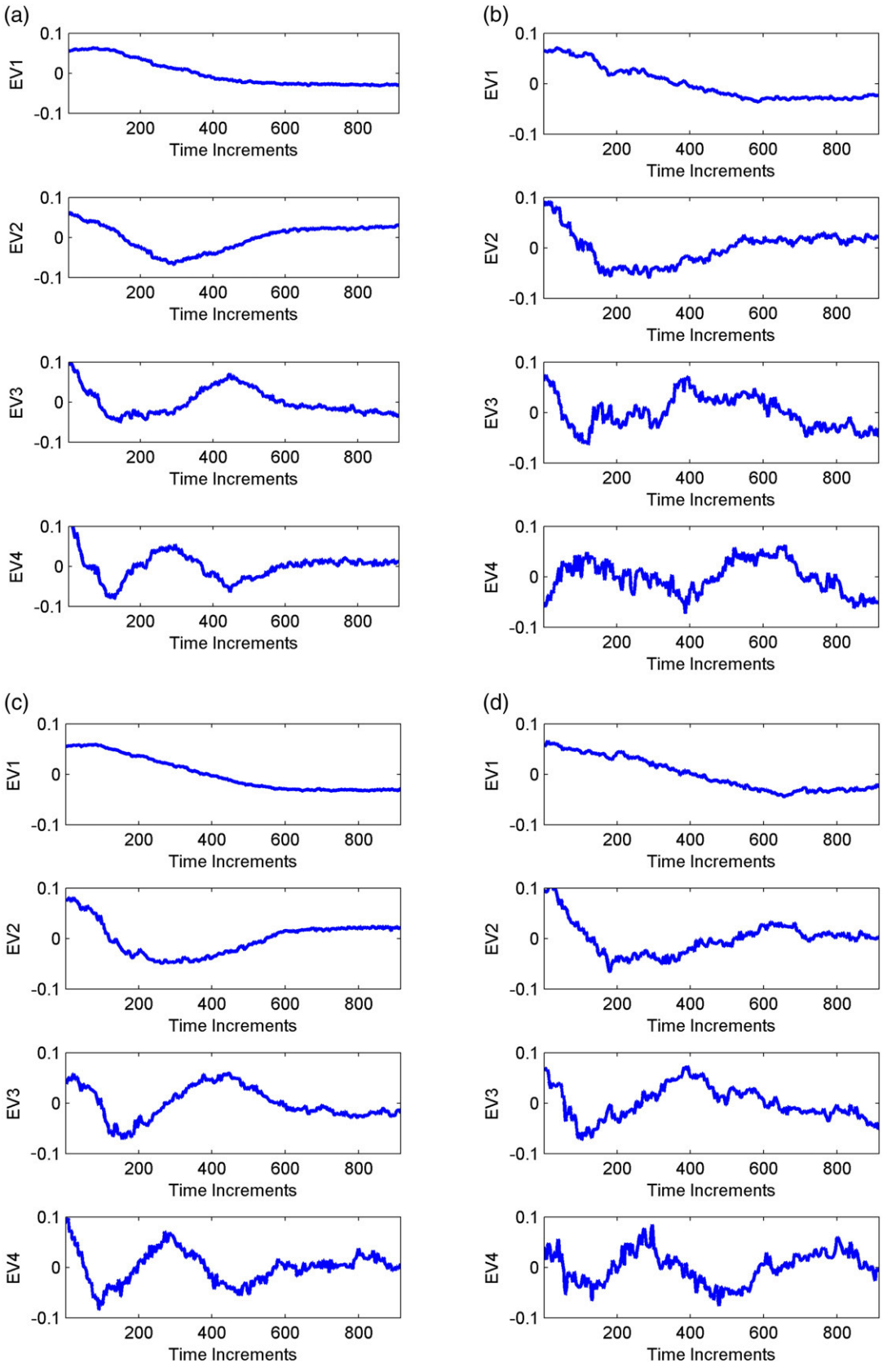

Fig. 16. Temporal amplitudes of the first four modes for each species in 3rd bilayer.

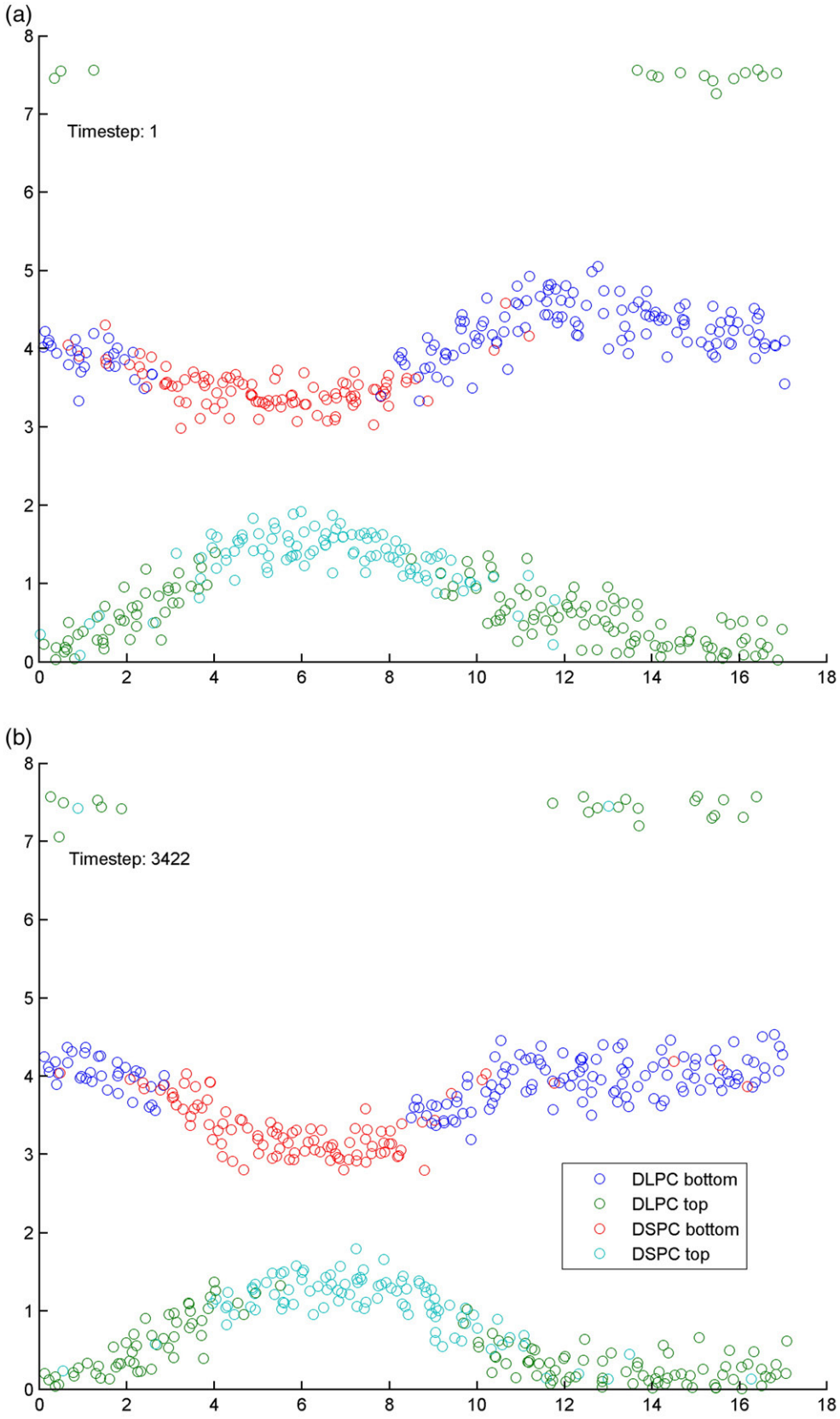

Fig. 17. Initial and final contour plots of the 4th bilayer system.

having an uneven concentration of lipids in each leaflet can lead to instability but that the two leaflets are coupled and their dynamics cannot be described independently. However, in system 3 we see also that bilayers are not perfectly coupled as even intermediate to large scale motions can occur in only one leaflet.

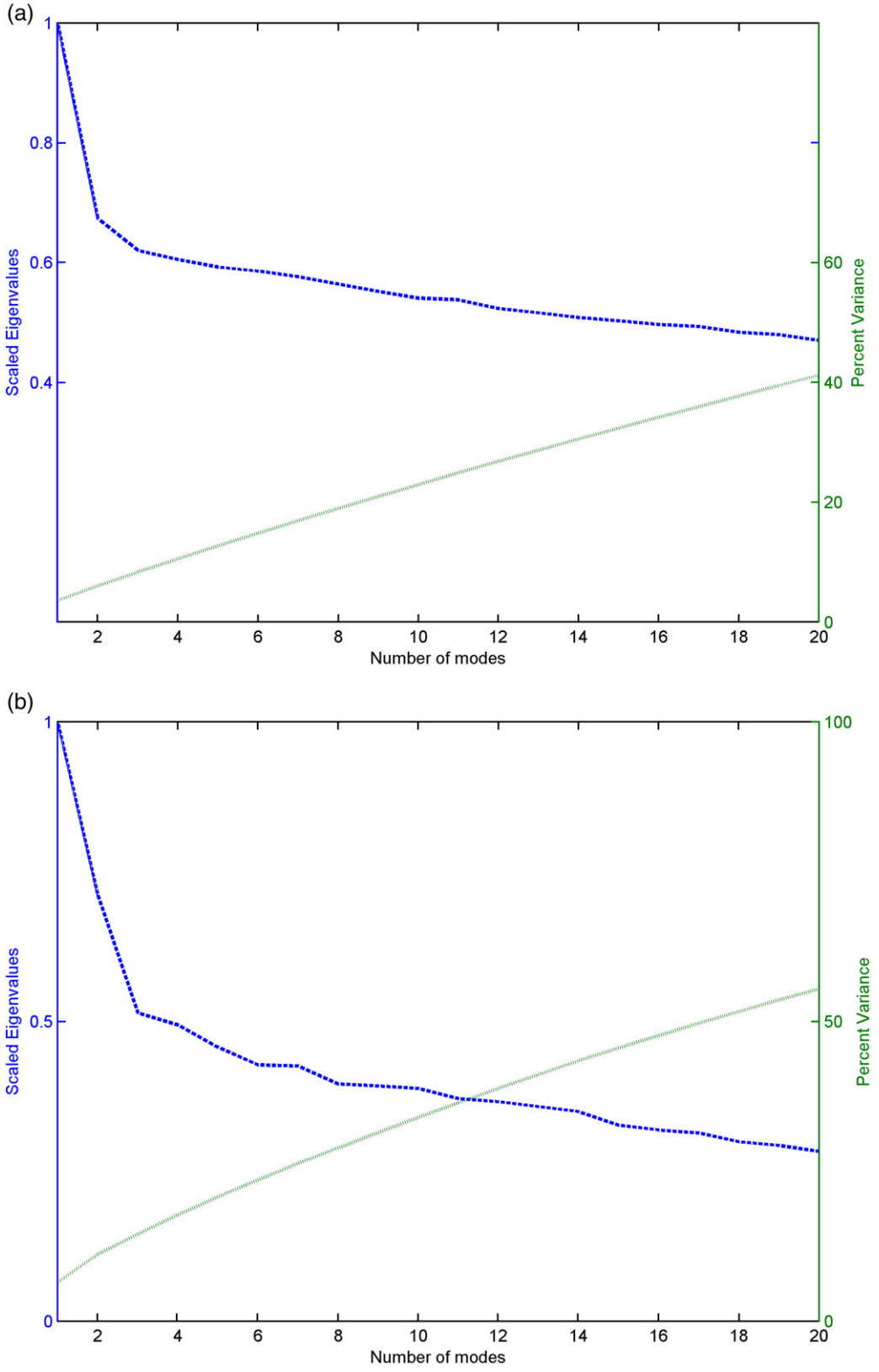

Fig. 18. Scree plots for both species in top layer.

For the stable system, we find many modes were needed to describe the changes taking place and that the majority of these changes took place internally within the phases of each respective lipid. This allows us to define a criterion of stability based on our expansion. A stable system does not exhibit a low-dimensional manifold describing the dynamics. This is different from principal

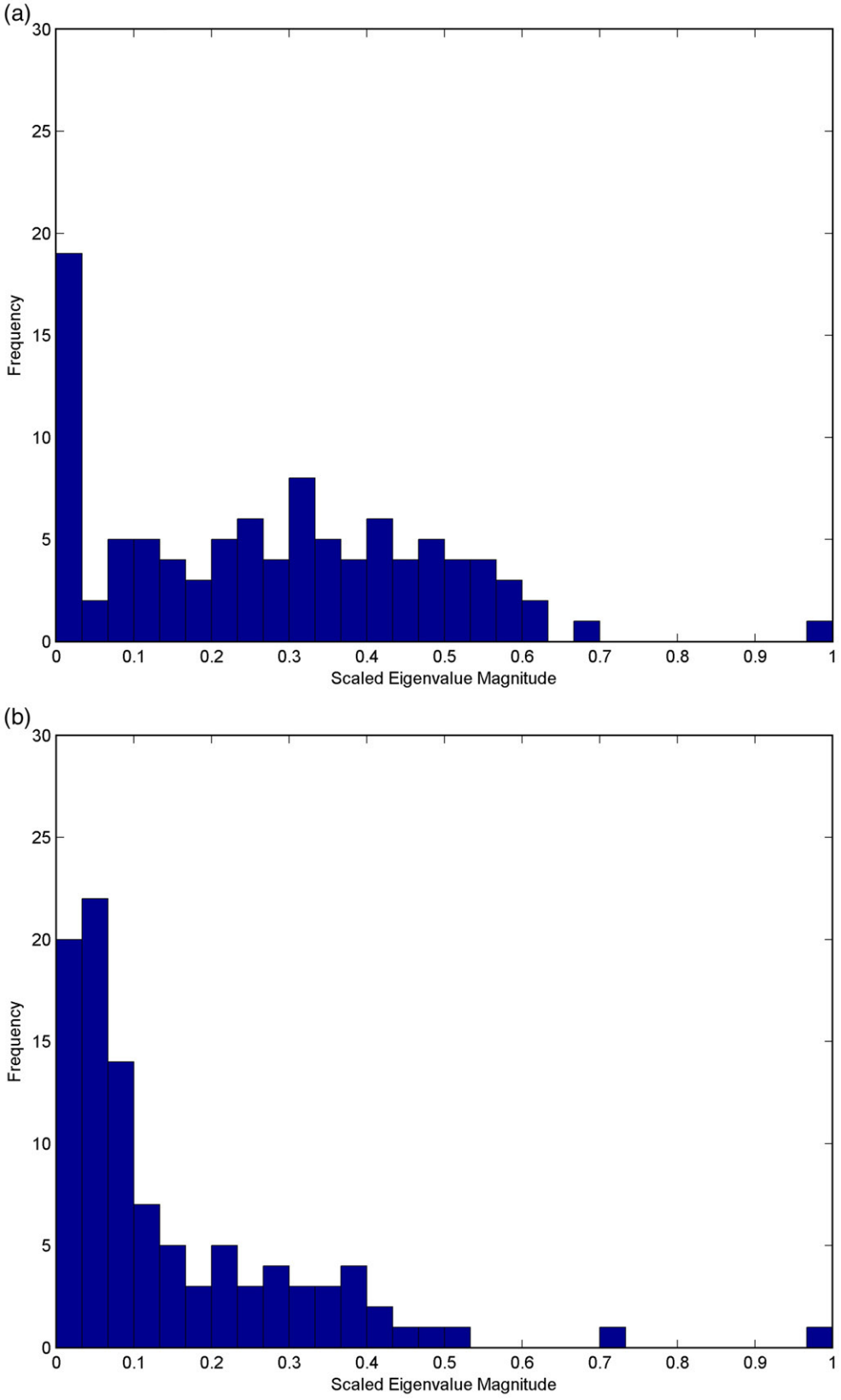

Fig. 19. Histogram plots of scaled eigenvalues for DSPC and DLPC on top layer.

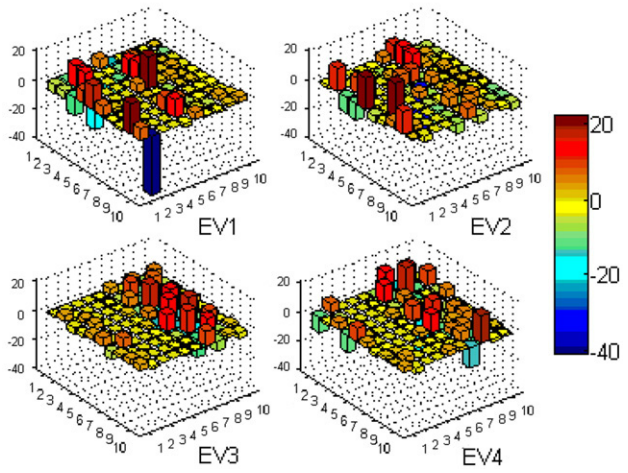

Fig. 20. Components of the first four modes for DLPC bottom.

component studies in protein dynamics where such a low-dimensional manifold typically can be used to find a small set of dynamic modes [33,35].

More data is needed to conclusively identify mechanisms that lead to decomposition of phase structures in bilayer systems. Instead of using density as the single parameter for KL expansion, we plan to use the deuterium order parameter averaged over gridspaces to identify changes in phase behavior. These results will be reported in the future.

Acknowledgement

We thank Sandra Bennun for providing us with simulation trajectories.

References

[1] R.B. Gennis, Biomembranes: Molecular Structure and Function, Springer, New York, 1989.
[2] P.L. Yeagle, Membranes of Cells, Academic Press, 1993.
[3] H.T. Tien, A. Ottova-Leitmannova, Planar Lipid Layers (BLM's) and Their Applications, Elsevier, Amsterdam, 2003.
[4] K. Simons, E. Ikonen, Functional rafts in cell membranes, Nature 387 (1997) 569–572.
[5] K. Simons, W.L.C. Vaz, Model systems, lipid rafts, and cell membranes, Annu. Rev. Biophys. Biomol. Struct. 33 (2004) 269–295.
[6] K. Simons, R. Ehehalt, Cholesterol, lipid rafts, and disease, J. Clin. Invest. 110 (2002) 597–603.
[7] E. Egberts, S.-J. Marrink, H.J.C. Berendsen, Molecular dynamics simulation of a phospholipid membrane, Eur. Biophys. J. 22 (1994) 423–436.
[8] S. Bennun, A.N. Dickey, C. Xing, R. Faller, Simulations of Biomembranes and Water: Important Technical Aspects, Fluid Phase Equilib. 261 (2007) 18–25.
[9] M. Patra, M. Karttunen, M. Hyvönen, E. Falck, P. Lindqvist, I. Vattulainen, Molecular dynamics simulations: major artifacts due to truncation of electrostatic interactions, Biophys. J. 84 (2003) 3636–3645.
[10] J. Aittoniemi, T. Róg, P. Niemela, M. Pasenkiewicz-Gierula, I. Vattulainen, M. Karttunen, Sterol tilt — major determinant of sterol ordering capability in lipid membranes, J. Phys. Chem., B (Letters) 110 (2006) 25562–25564.
[11] D.P. Tieleman, D. van der Spoel, H.J.C. Berendsen, Molecular dynamics simulations of dodecylphosphocholine micelles at three different aggregate sizes: micellar structure and chain reaction, J. Phys. Chem., B 104 (2000) 6380–6388.
[12] M. Bachar, P. Brunelle, D.P. Tieleman, A. Rauk, Molecular dynamics simulation of polyunsaturated lipid bilayer susceptible to lipid peroxidation, J. Phys. Chem., B 108 (2004) 7170–7179.
[13] K. Tu, M.L. Klein, D.J. Tobias, Constant-pressure molecular dynamics investigation of cholesterol effects in a dipalmitoylphosphatidylcholine bilayer, Biophys. J. 75 (1998) 2147–2156.
[14] A.K. Sum, R. Faller, J.J. de Pablo, Molecular simulation study of phospholipid bilayers and insights of the interactions with disaccharides, Biophys. J. 85 (2003) 2830–2844.
[15] A.N. Dickey, R. Faller, How alcohol chain-length and concentration modulate hydrogen bond formation in a lipid bilayer, Biophys. J. 92 (2007) 2366–2376.
[16] S.V. Bennun, M.L. Longo, R. Faller, Phase and mixing behavior in two-component lipid bilayers: a molecular dynamics study in DLPC/DSPC mixtures, J. Phys. Chem., B 111 (2007) 9504–9512.
[17] S.J. Marrink, A.H. de Vries, A.E. Mark, Coarse grained model for semi-quantitative lipid simulation, J. Phys. Chem., B 108 (2004) 750–760.
[18] S.J. Marrink, H.J. Risselada, S. Yefimov, D.P. Tieleman, A.H. de Vries, The MARTINI Force Field: coarse grained model for biomolecular simulations, 111 (2007) 7812–7824.
[19] C.F. Lopez, S.O. Nielsen, P.B. Moore, J.C. Shelley, M.L. Klein, Self-assembly of a phospholipid Langmuir monolayer using coarse-grained molecular dynamics simulations, J. Phys., Condens. Matter 14 (2002) 9431–9444.
[20] G. Brannigan, F.L.H. Brown, Solvent-free simulations of fluid membrane bilayers, J. Chem. Phys. 120 (2004) 1059–1071.
[21] O. Farago, "Water-free" computer model for fluid bilayer membranes, J. Chem. Phys. 119 (2003) 596–605.
[22] B.J. Reynwar, G. Illya, V.A. Harmandaris, M.M. Müller, K. Kremer, M. Deserno, Aggregation and vesiculation of membrane proteins by curvature-mediated interactions, Nature 447 (2007) 461–467.
[23] I.R. Cooke, K. Kremer, M. Deserno, Tunable generic model for fluid bilayer membranes, Phys. Rev., E 72 (2005) 011506.
[24] J.E. Jackson, A User's Guide to Principal Components, Wiley-Interscience, New York, 1991.
[25] L. Sirovich, R. Everson, Management and analysis of large scientific datasets, Int. J. Supercomput. Appl. High Perform. Comput. 6 (1992) 50–68.
[26] J. Switzer, S. Bennun, M.L. Longo, A. Palazoglu, R. Faller, Karhunen-Loeve analysis for pattern description in phase separated lipid bilayer systems, J. Chem. Phys. 124 (2006) 234906.
[27] S. Bennun, M.L. Longo, R. Faller, The Molecular scale structure in fluid–gel patterned bilayers: stability of interfaces and transmembrane distribution, Langmuir 23 (2007) 12465–12468.
[28] E. Lindahl, B. Hess, D. van der Spoel, GROMACS 3.0: a package for molecular simulation and trajectory analysis, J. Mol. Model. 7 (2001) 306–317.
[29] W. Lin, C. Blanchette, T.V. Ratto, M.L. Longo, Lipid asymmetry in DLPC/DSPC supported lipid bilayers: a combined AFM and fluorescence microscopy study, Biophys. J. 90 (2006) 228–237.
[30] S. Mabrey, J.M. Sturtevant, Investigation of phase transitions of lipids and lipid mixtures by high sensitivity differential scanning calorimetry, Proc. Natl. Acad. Sci. U. S. A. 73 (1976) 3862–3866.
[31] H.J.C. Berendsen, J.P.M. Postma, W.F. van Gunsteren, A. DiNola, J.R. Haak, Molecular dynamics with coupling to an external heat bath, J. Chem. Phys. 81 (1984) 3684–3690.
[32] R.W. Preisendorfer, Principal Component Analysis in Meteorology and Oceanography, Elsevier, Amsterdam, 1988.
[33] S.A.M. Stein, A.E. Loccisano, S.M. Firestine, J.D. Evanseck, Principal components analysis: a review of its application on molecular dynamics data, Ann. Rep. in Comp. Chemistry 2 (2006) 233–261.
[34] R. Faller, S.-J. Marrink, Simulation of domain formation in mixed DLPC-DSPC lipid bilayers, Langmuir 20 (2004) 7686–7693.
[35] B. Hess, Similarities between principal components of protein dynamics and random diffusion, Phys. Rev. E 62 (2000) 8438–8448.

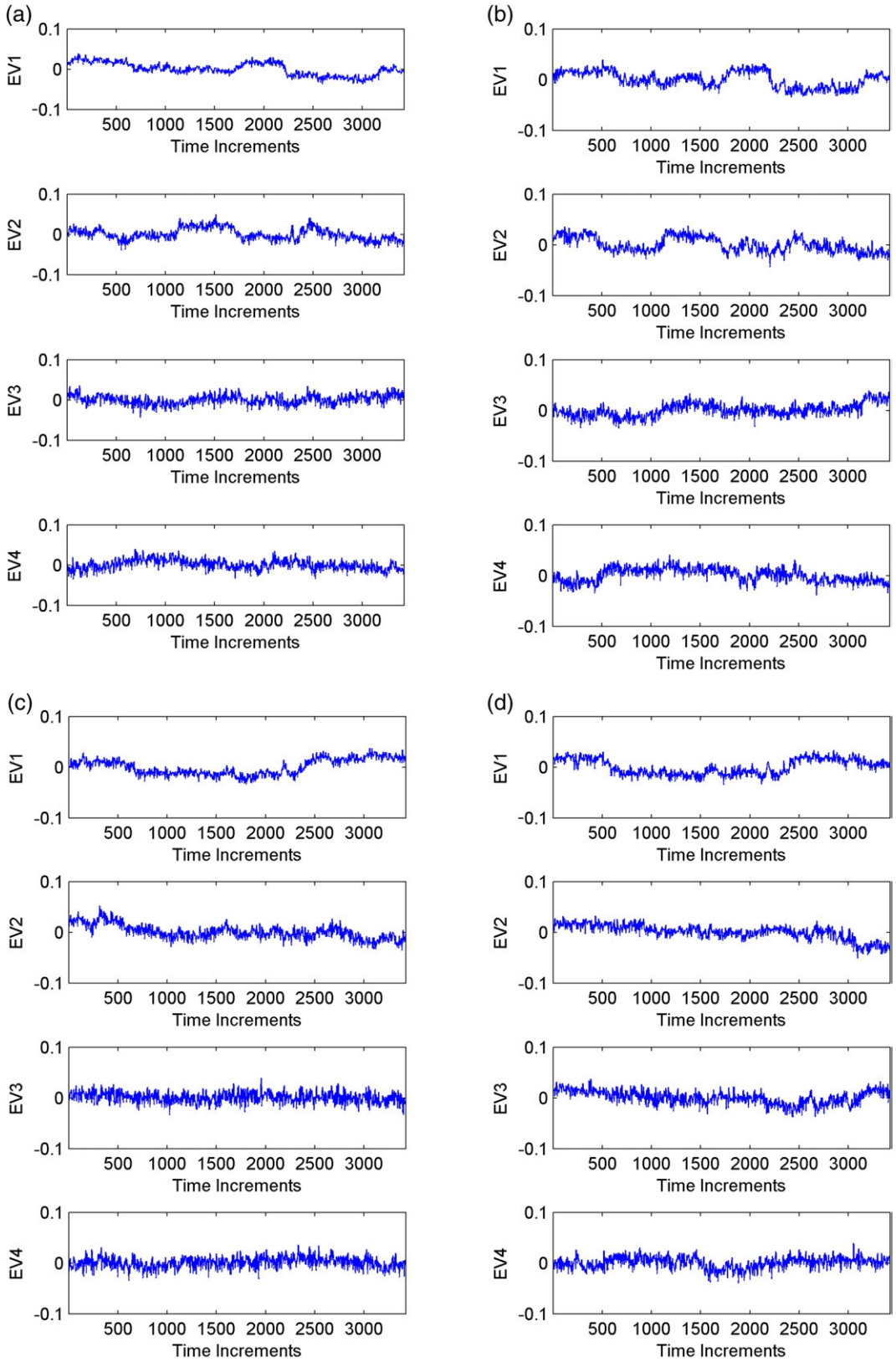

Fig. 21. Temporal amplitudes for the first four modes in fourth bilayer.